JGR Solid Earth

RESEARCH ARTICLE
10.1029/2020JB019405

Seismo-Turbidites in Aysén Fjord (Southern Chile) Reveal a Complex Pattern of Rupture Modes Along the 1960 Megathrust Earthquake Segment

Katleen Wils[1], Maarten Van Daele[1], Catherine Kissel[2], Jasper Moernaut[3], Sabine Schmidt[4], Giuseppe Siani[5], and Galderic Lastras[6]

[1]Renard Centre of Marine Geology (RCMG), Department of Geology, Ghent University, Ghent, Belgium, [2]Laboratoire des Sciences du Climat et de l'Environnement/IPSL, CEA/CNRS/UVSQ, Université Paris-Saclay, Gif-sur-Yvette, France, [3]Institute of Geology, University of Innsbruck, Innsbruck, Austria, [4]EPOC, UMR CNRS 5805, Université de Bordeaux, Pessac, France, [5]GEOPS, UMR 8148 Université de Paris, Orsay, France, [6]GRC Geociències Marines, Universitat de Barcelona, Barcelona, Spain

Key Points:
- Oldest evidence for megathrust earthquakes in southern Chile
- Confirmation of variable rupture model and first evidence for 1960-like full-segment ruptures along the Valdivia segment
- Different rupture types influence full-segment rupture recurrence rates

Supporting Information:
- Supporting Information S1
- Table S1
- Table S2
- Table S3

Correspondence to:
K. Wils,
katleen.wils@ugent.be

Citation:
Wils, K., Van Daele, M., Kissel, C., Moernaut, J., Schmidt, S., Siani, G., & Lastras, G. (2020). Seismo-turbidites in Aysén Fjord (southern Chile) reveal a complex pattern of rupture modes along the 1960 megathrust earthquake segment. *Journal of Geophysical Research: Solid Earth*, *125*, e2020JB019405. https://doi.org/10.1029/2020JB019405

Received 12 JAN 2020
Accepted 28 AUG 2020
Accepted article online 3 SEP 2020

Abstract Grainsize analysis and end-member modeling of a long sediment core from Aysén Fjord (southern Chile) allows to identify over 25 seismo-turbidites in the last 9,000 years. Considering the shaking intensities required to trigger these turbidites (V½-VI½), the majority can be related to megathrust earthquakes. Multiple studies in south-central Chile have aimed at finding traces of giant, tsunamigenic megathrust earthquakes leading to the current 5,500-year-long paleoseismological record of the Valdivia segment. However, none of these cover the southern third of the segment. Aysén Fjord allows to fill this data gap and presents the first, crucial paleoseismic data to demonstrate that the 1960 event was not unique for the Valdivia segment, yielding a recurrence rate of 321 ± 116 years in the last two millennia. Moreover, the oldest identified events in Aysén Fjord date back to 9,000 cal years BP and, thus, also extend the regional paleoseismological record in time. We infer a large temporal variability in rupture modes, with successions of full-segment ruptures alternating with partial and cascading ruptures. The latter seems to significantly postpone the occurrence of another full rupture when consecutively occurring in different parts of the segment. Additionally, one outstanding period of seismic quiescence —during which no megathrust earthquake evidence has been found at any paleoseismic site—occurred after a full rupture in AD ~745 that presents an unusual uplift/subsidence pattern. Such variability makes it highly speculative to anticipate the rupture mode of the next megathrust earthquake along the Valdivia segment.

1. Introduction

One of the key aspects for reliable seismic hazard assessment is the understanding of earthquake recurrence patterns in time and space. This is especially true for areas that are prone to high-magnitude earthquakes, typically associated to large subduction zones such as those at the Peru-Chile Trench, the Alaska-Aleutian Megathrust, the Nankai Trough in Japan, the Sunda Megathrust in Indonesia, or the Cascadia Subduction zone along the western coast of the USA (Satake & Atwater, 2007). Multiple studies have attempted to reveal past earthquake events in these seismically active regions by studying a variety of natural archives such as lakes, fjords, coastal marshes, and continental margins. Common examples are studies of turbidites and/or mass-transport deposits (MTDs) present in both lacustrine (e.g., Moernaut et al., 2018; Praet et al., 2017) and offshore environments (e.g., Goldfinger et al., 2003; Kuehl et al., 2017) and the search for tsunami deposits (e.g., Kempf et al., 2017; Komatsubara & Fujiwara, 2007) or biological and sedimentological indicators for coseismic elevation changes (e.g., Garrett et al., 2015; Philibosian et al., 2017) in coastal areas.

Being one of the most seismically active regions in the world with a variety of natural archives, south-central Chile has been the research topic in a considerable number of paleoseismological studies with a focus on the Valdivia segment (e.g., Cisternas et al., 2005; Kempf et al., 2017; Moernaut et al., 2018; St-Onge et al., 2012). This is easy to understand considering that this segment ruptured in 1960 with an M_w of 9.5, making it the largest instrumentally recorded earthquake worldwide (Lomnitz, 2004). Historical documents show that at least 3 other $M_w \geq 7$–8 events occurred in the 1960 earthquake region in the last ~400 years (Lomnitz, 2004).

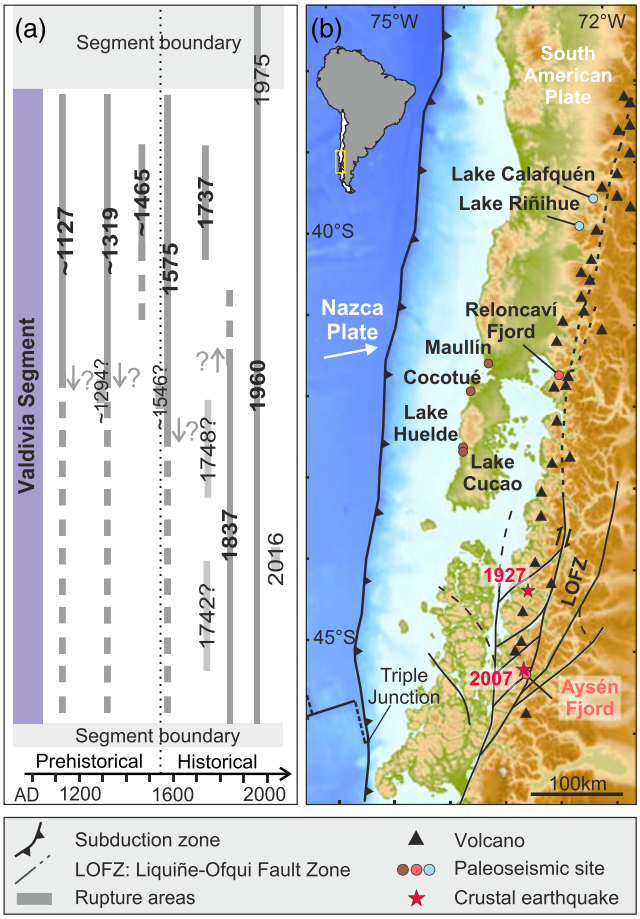

Figure 1. Geological setting of Aysén Fjord and the Valdivia segment. (a) Approximate rupture areas for megathrust earthquakes along the Valdivia segment of the Chilean subduction zone during the last millennium as proposed by Cisternas, Garrett, et al. (2017), Moernaut et al. (2014), and Moernaut et al. (2018) based on instrumental, historical, and paleoseismic data. (b) Tectonic setting of south central Chile with location of Aysén Fjord within the Liquiñe-Ofqui Fault Zone (LOFZ) and along the Valdivia segment. Red stars represent epicenters of historical crustal earthquakes in 2007 (M_w 6.2; Naranjo et al., 2009) and 1927 (M 7.1; Naranjo et al., 2009). Colored dots are the location of published paleoseismic records considered in this research, including coastal records of coseismic subsidence and tsunamis (brown) and turbidite records in fjords (pink) and lakes (blue). Black triangles are Holocene and/or historically active volcanoes. Figure adapted from Moernaut et al. (2018).

Combining different studies in south-central Chile allowed for a regional paleoseismic record to be composed that dates back to about 3,700 years and shows quasi-periodic occurrence of $M_w \geq 8.6$ earthquakes (Moernaut et al., 2018), whereas single archives date back to maximum 5,500 years (Kempf et al., 2017). Several of these megathrust earthquakes are assumed to have also ruptured the southern third of the Valdivia segment—resulting in a full rupture—but there are currently no paleoseismological studies covering this section. This leaves a gap in our knowledge of the southern extent of past ruptures and thus significant uncertainty on the interpretation of paleo-earthquakes being 1960-like full-segment ruptures. Therefore, it is not clear how often partial ruptures (M_w ~8 events) occur compared to full ruptures and thus their relative importance for accommodating slip deficit in the Valdivia segment remains elusive. Here we present a record of past megathrust earthquakes based on the occurrence of seismo-turbidites in a long sediment core retrieved from Aysén Fjord, located along the southern third of the Valdivia segment. This study extends the spatial coverage of the currently available paleoseismic record, revealing recurrence patterns with much higher certainty. Additionally, it dates back to ~9,000 cal years BP, making it the longest record of past megathrust earthquakes on the Valdivia segment that is currently available.

2. Setting

2.1. Seismotectonic Characterization of South-Central Chile

Oblique subduction of the Nazca Plate under the South American Plate is the dominant process that controls the tectonic setting of Chile. It results in the presence of a subduction megathrust, reaching all the way south to the Triple Junction (Figure 1b). Different seismotectonic segments can be distinguished based on records of historical earthquakes (Métois et al., 2012). Aysén Fjord is located along the southernmost segment referred to as the Valdivia segment (~38–46°S; Figure 1a). Several hypotheses have been raised to explain what controls its northern limit, including low interplate coupling as a result of subducted positive-relief structures (Geersen et al., 2013; Moreno et al., 2011; Sparkes et al., 2010), the presence of a discontinuity in the continental basement (Melnick et al., 2009) or splay faults that take up part of the plate convergence (Moreno et al., 2012). The 1960 Great Chilean Earthquake can be considered diagnostic for the extent of the Valdivia segment (Figure 1a). This tsunamigenic earthquake ruptured the entire 1,000 km length of the segment in one single event with the largest instrumentally recorded magnitude (M_w 9.5) to date (Cifuentes, 1989). Additionally, it remains the only confirmed full-segment rupture of the Valdivia segment. Most of the slip (locally reaching more than 40 m) during this event was accommodated in the northern half of the segment, but over 20 m of maximum slip still occurred at the latitude of Aysén Fjord (Moreno et al., 2009). Estimated seismic shaking intensities in the Aysén Fjord region vary from IV (Lazo Hinrichs, 2008) to VI-VI½ (USGS, 2018).

To accommodate for the oblique component of subduction, a dextral strike-slip fault system (Liquiñe-Ofqui Fault Zone, LOFZ; Figure 1b) stretches across northern Patagonia with several fault branches intersecting Aysén Fjord (Mora et al., 2010). The most significant recent crustal earthquake in the region occurred in April 2007 (M_w 6.2) as part of a seismic swarm and had its epicenter in the fjord. Intensities in the epicentral area ranged from VIII to IX and rapidly decreased to VII on the eastern extremity of the fjord in the Aysén River Delta area (Figure 2) (Naranjo et al., 2009). As a result, hundreds of mass movements were triggered

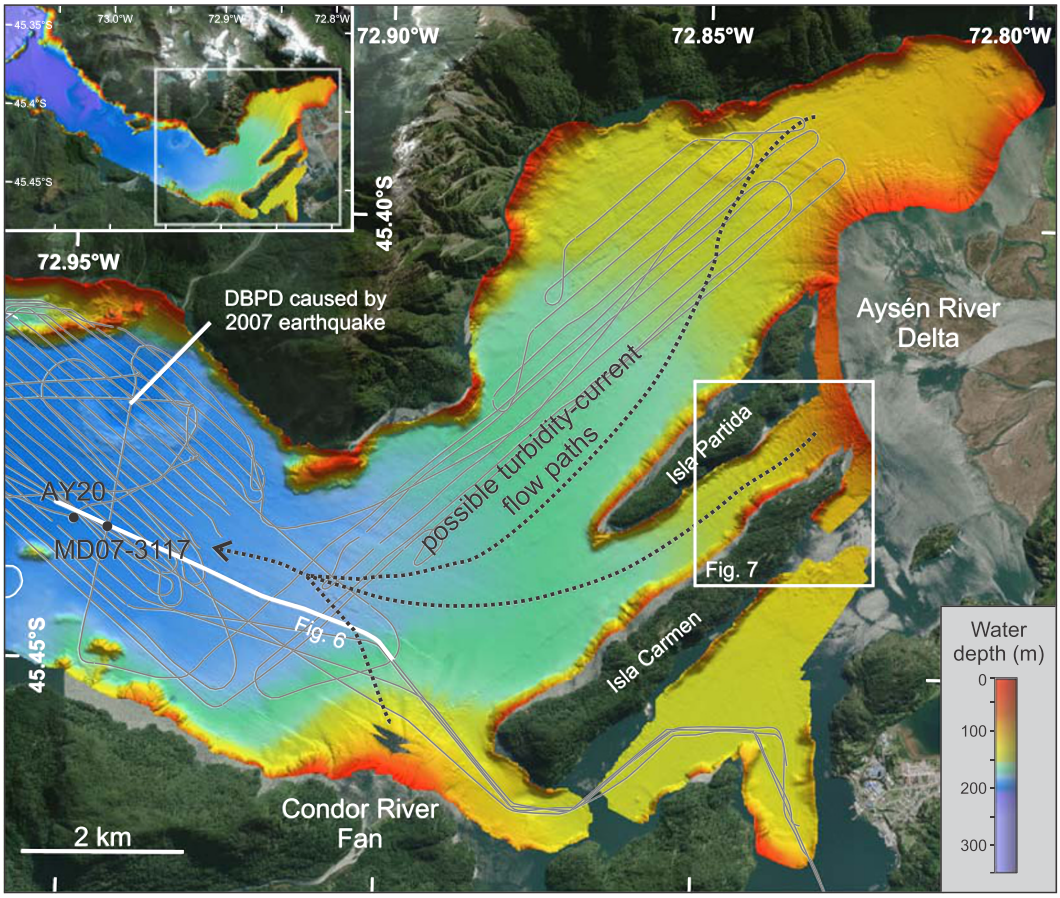

Figure 2. Multibeam bathymetry map (ELAC SeaBeam 1050) of the easternmost part of Aysén Fjord plotted on a satellite image (©DigitalGlobe) of the area. Core locations of AY20 and MD07-3117 are indicated (black dots), as well as TOPAS (Kongsberg TOPAS PS18 parametric subbottom profiler) seismic profile lines (gray lines, white for the section shown in Figure 6). More information concerning geophysical data acquisition and processing can be found in Wils et al. (2018). The MD07-3117 core studied here was retrieved 2 months prior to the 2007 earthquake, which generated the deformed basin-plain deposit (DBPD) that can be observed to the north-northeast of the coring location (cf. Van Daele et al., 2013). Dotted lines indicate possible flow paths for turbidity currents originating from the Aysén River Delta in the east or the Condor River Fan in the south. A zoom to the turbidite sediment source area between Isla Partida and Isla Carmen is presented in Figure 7.

along the fjord's coastline (Naranjo et al., 2009) resulting in a tsunami in the fjord killing 10 persons (Lastras et al., 2013). Another historical event took place in November 1927 just over 100 km north of the fjord (Figure 1b). This event had an estimated magnitude of 7.1 and caused large mass movements and tsunamis in the nearby fjords and thus appears similar to the 2007 earthquake in Aysén Fjord (Naranjo et al., 2009).

2.2. A Regional Record of Megathrust Earthquakes

Apart from the 1960 earthquake, historical records document three significant megathrust earthquakes in south-central Chile with magnitudes exceeding 7.5, in AD 1575, 1737, and 1837 (Figure 1a) (Lomnitz, 2004). Our current knowledge of prehistorical events is based on a compilation of sedimentary records covering the last 5,500 years with a focus on the last millennium, including coastal evidence for coseismic elevation changes and tsunamis (e.g., Cisternas et al., 2005; Ely et al., 2014; Garrett et al., 2015; Kempf et al., 2017, 2020) and subaqueous turbidites in lakes and fjords (Moernaut et al., 2014, 2018; St-Onge et al., 2012). Although there are local differences between these records in terms of the number of recorded earthquakes and their recurrence intervals, they all point to a variable rupture mode along the Valdivia segment (Cisternas, Garrett, et al., 2017; Moernaut et al., 2014) including local, single-asperity ruptures with M_w generally around 7–8 as well as multiasperity ruptures affecting large portions (>300 km) of the segment and reaching an M_w of 8.6 or higher (Moernaut et al., 2018). These long

ruptures can also show different lengths (e.g., AD 1837 and 1960), indicating that there is more variability than just small and large ruptures (Moernaut et al., 2014).

As most of the studied paleoseismic localities in south-central Chile show evidence for the CE 1575 event, Moernaut et al. (2014) and Cisternas, Garrett, et al. (2017) interpret this earthquake as a 1960-like full rupture, despite lacking any record in the southern third of the Valdivia segment. Similarly, they assume a full-rupture mode for the AD ~1319 and ~1127 events. A rupture of the southern half of the Valdivia segment occurred in AD 1837, although the limit of its northern extent could not yet be determined (Moernaut et al., 2014). Smaller partial ruptures took place in AD 1737 and ~1465, all in the northern third of the segment (Cisternas, Garrett, et al., 2017; Moernaut et al., 2014). This shows that high-magnitude earthquakes rupturing large portions of the subduction zone as well as smaller earthquakes with less extensive rupture dimensions take place at variable recurrence rates. Moernaut et al. (2014) infer an average recurrence time of 280 years for 1960-like earthquakes and 140 years when also including smaller ruptures. A single-asperity rupture occurred during the 2016 Chiloé earthquake (Melgar et al., 2017). Cisternas, Garrett, et al. (2017) advocate for additional local events in AD 1546 and 1294. Several earthquakes were also reported in the southern part of the Valdivia segment in the years following the 1737 event, such as in 1742 and 1748, but their characteristics are unknown (Lomnitz, 2004).

The number of records covering the period before AD 1000 is limited. Nevertheless, the average recurrence rate of about 280 years remains stable when including the preceding 1,000 years of earthquakes found by Cisternas et al. (2005) in coastal marshes in the central third of the Valdivia segment. Most of these events show similar subsidence and tsunami evidence as the 1960 earthquake and are therefore considered as 1960-like giant megathrust events (Cisternas et al., 2005), although their actual rupture length cannot be resolved. Moernaut et al. (2018) confirm this hypothesis and update the average recurrence rate to 292 ± 93 years (coefficient of variation, CoV, 0.32) for $M_w \geq 8.6$ events in the last 3,600 years. For earthquakes with $M_w \geq 7.7$, the shorter average recurrence time of ~140 years is maintained for the last 5,000 years and revised to 139 ± 69 years (CoV 0.5). In both cases, megathrust earthquakes thus show quasi-periodic time-dependent recurrence behavior although smaller events appear to occur less periodically than the giant ones (Moernaut et al., 2018). Important temporal variability is also observed for tsunami recurrence at the central third of the Valdivia segment (Kempf et al., 2019), where the average recurrence interval of 325 years actually coincides with a minimum in the recurrence distribution.

2.3. Aysén Fjord as Paleoseismic Recorder

Previous research in Aysén Fjord (Van Daele et al., 2013; Vanneste et al., 2018; Wils et al., 2018) has shown that its sediments are a valuable archive for paleoseismological research, with a particular focus on crustal earthquakes due to its location on the LOFZ (Figure 1b). Traces of the 2007 Aysén earthquake were identified on high-resolution bathymetric and seismic data covering the inner part of the fjord, together with nine older seismic-stratigraphic levels (termed SL-A, SL-B, SL-C, SL-CD, SL-D, SL-DE, SL-EF, SL-F, and SL-G) characterized by the presence of seismically triggered MTDs related to fjord wall collapses and/or subaqueous landslides (Van Daele et al., 2013; Wils et al., 2018). Age ranges for these MTDs were provided by a 21 m long, radiocarbon-dated sediment core (MD07-3117, collected 2 months before the 2007 earthquake) through correlation of the mapped MTD-levels with turbidites in the core (Wils et al., 2018). Forward modeling of seismic shaking intensities to match observed MTD distributions by considering the threshold values required to trigger different MTD types allowed to confirm that the majority of these MTDs are generated by crustal earthquakes on the LOFZ but can in some cases (i.e., for SL-EF and SL-DE) also result from megathrust earthquakes as no definite LOFZ source can be identified (Vanneste et al., 2018). Additionally, a megathrust-related origin for SL-EF was suggested by Wils et al. (2018) as well by considering its MTD sizes, distribution and age overlap with a megathrust earthquake between AD ~ −50 and 50 known from another paleoseismic site (Kempf et al., 2017).

In the inner part of the fjord, some pulses in the seismo-turbidite resulting from the 2007 earthquake consist of dark-gray to black volcanic sandy material (Van Daele et al., 2013). This material originates from the Aysén River Delta (Figure 2) as shown by reconstructed flow directions and because the fjord walls have a granitic to dioritic composition and thus produce much lighter-colored turbidites (Sernageomin, 2002; Van Daele et al., 2014). Moreover, their magmatic origin is illustrated by high values of magnetic susceptibility (MS) and radiodensity (Van Daele et al., 2014). Shaking intensities ≥ V½ are assumed to trigger delta

failures in Chilean lakes along the Valdivia segment (Moernaut et al., 2014). Similar values of V¼–V½ are reported in Alaskan lakes (Van Daele, Haeussler, et al., 2019), also located in a high-seismicity setting. Therefore, we can assume that ~V½ can be considered as a general threshold for delta failures in these settings and can thus also be applied in Aysén Fjord (cf. Vanneste et al., 2018). Both of the deposits that are possibly resulting from a megathrust earthquake (SL-EF and SL-DE) are characterized by this type of deltaic turbidite, as well as small-scale offshore MTDs (seismic intensity ≥ VI½; Vanneste et al., 2018) near the vertical resolution limit of the reflection-seismic data (Wils et al., 2018). More megathrust-earthquake-related deposits might thus be present in the fjord infill that remain undetected on the seismic profiles but could potentially be revealed by the presence of turbidites in the sediment core.

3. Material and Methods

To uncover possible megathrust-earthquake related turbidites, we present a thorough analysis of the same long sediment core that was used by Wils et al. (2018). The MD07-3117 core was retrieved in the inner part of Aysén Fjord during the MD159-PACHIDERME cruise on board the R.V. *Marion Dufresne* (Figure 2). It consists mostly of brown hemipelagic mud, intercalated by event deposits such as tephras and turbidites (Wils et al., 2018). Due to strong bioturbation, a combination of core pictures, magnetic properties, CT images, and grain size analysis is required to unambiguously identify turbidites in the core.

The sediment core was logged with the Geotek Multi-Sensor Core Logger at Ghent University to obtain digital linescan images and high-resolution MS measurements every 2 mm using a Bartington MS2E point sensor. Changes in magnetite grain size are determined by the ratio ARM/κ, where ARM is the anhysteretic remanent magnetization, obtained by applying a 100 mT alternating field and a 50 μT bias field, and κ is the volume low-field MS. Both were measured on u-channels in the shielded room of the Laboratoire des Sciences du Climat et de l'Environnement (France). Subsequently, the archive half was CT scanned at the Ghent University Hospital (Siemens; SOMATOM Definition Flash; Siemens AG). Each scan has a ~0.2 mm resolution in the x and y directions and a z resolution of either 0.3 or 0.6 mm. VGStudio 3.2 and ImageJ software were used for visualization and analysis, respectively. Layers that appear anomalous on the core pictures or show elevated values in MS and/or radiodensity (expressed in Hounsfield Units, HU) were considered as potential turbidites and some smear slides were made to show their composition. Each of these layers was sampled for grain size analysis with the Malvern Mastersizer 3000 after removal of organic matter, calcium carbonate and biogenic silica (after Van Daele et al., 2016). Due to strong bioturbation in the core, at least three samples—covering a depth of 0.5 cm per sample—were taken in each interval when possible, to make sure that the potential turbidite was adequately sampled. Some samples of background sedimentation and turbidites previously described by Wils et al. (2018) were also analyzed for comparison. Samples in background sedimentation were only taken in homogenous areas where no significant changes in MS occur and at least 5 cm above or below a possible turbidite. In total, 12 of these samples were taken spread over the entire length of the core. The MATLAB-based software tool AnalySize (version 1.0.2) was used to distinguish different grain size populations by applying parametric Weibull distributions (Paterson & Heslop, 2015).

To allow for detailed comparison of Aysén's turbidite record to other paleoseismological studies along the Valdivia segment, the age model established by Wils et al. (2018) was refined by radiocarbon dating 25 additional samples of organic macroremains (leaves, twigs, and seeds) in the top sections of the core (Table S3 in the supporting information). Analyses were done at the ARTEMIS accelerator mass spectrometry (AMS) facility in Saclay. Some very small samples were measured in a specific batch with matching size-normalizing standards and optimized source setup (Delqué-Količ et al., 2013). A mass-dependent background correction was applied to all samples. Radiocarbon ages were calculated according to the procedure described by Mook and van der Plicht (2016) and calibrated using SHCal13 (Hogg et al., 2013). Age-depth modeling was done with Bacon (Blaauw & Christen, 2011), an R package that uses Bayesian statistics to obtain a suitable age model. To verify whether the top sediments were recovered during the piston coring process, the studied sequence of MD07-3117 was correlated to a short gravity core (AY20) retrieved nearby (Figure 2) and studied by Van Daele et al. (2014). Core AY20 was recovered in 2009 and contains a turbidite at the top that was deposited during the April 2007 earthquake and is thus considered to be complete. A tephra layer present in both cores was sampled and analyzed for its major-element composition on the

CAMECA-SX Five Electron Microprobe (EPMA-CAMPARIS) at the University Paris VI (France) to verify the correlation. Additionally, geochemical data allowed the volcanic source to be identified and, in this way, validate the age-depth model.

As the most recent giant earthquake along the Valdivia segment occurred post-1950, and thus after the time-frame suitable for classical radiocarbon dating, the age-depth model was completed by short-lived radionuclide dating (^{210}Pb and ^{137}Cs) of the uppermost part of the AY20 core. Core AY20 was preferred to MD07-3117 because the exact age of the uppermost sediments of the latter is unclear due to strong piston coring-related deformation. Once both cores were correlated, the ^{210}Pb-based ages were used to verify the radiocarbon-based ages of the MD07-3117 core. Selected samples were freeze-dried and ^{210}Pb, ^{226}Ra, and ^{137}Cs activities were measured using a well-shaped γ-detector (CANBERRA) at the University of Bordeaux. Calibration of the detector was achieved using certified reference materials (IAEA-RGU-1; SOIL-6). Measured activities are expressed in mBq/g and errors were calculated based on 1 standard deviation counting statistics. The excess activity of ^{210}Pb ($^{210}Pb_{xs}$, used to calculate sediment ages) was determined by subtracting ^{226}Ra from the total measured ^{210}Pb activity.

4. Results

4.1. Turbidite Identification

The grain size distributions of 190 samples taken in 64 different intervals in the core were analyzed (Table S1). Combination of all grain size data shows four unimodal grain size populations (end-members, EMs) with limited overlap that explain ~98% of the variation in the dataset (Figure 3a). To confidently identify the origin of each EM, samples taken in turbidites described by Wils et al. (2018) and background sediments were analyzed as well. Grain size analysis of these calibration samples shows that the fine-grained silty population (EM1) appears to dominate in the background samples, while the three additional coarser-grained end-members are strongly present in the turbidite samples (EM2, EM3, and EM4, modes 25.75, 81.2, and 376 μm, respectively). This shows that grain size analysis can be used to distinguish event sedimentation from the normal, steady state background sedimentation in the fjord. The background samples have an average EM1 content of ~85% with an error (2σ) of 12%. This means that all unknown samples consisting of less than 73% EM1 cannot be background sediment (with 95% certainty) and are part of some sort of event deposit. A total of 28 intervals are interpreted as background sediments. The remaining 36 sampled intervals contain at least one sample containing less than 73% of EM1 and are therefore considered as event deposits. The applied procedure to determine whether or not a specific interval can be considered as a seismo-turbidite is schematically presented in Figure 3c (see also Table S2).

4.2. Classification and Interpretation of the Turbidite Record

To further classify the event deposits, of which a few are visualized in Figure 4, we consider that seismo-turbidites in Aysén Fjord are characterized by an elevated radiodensity and MS that reflects their magmatic mineral content (cf. short cores analyzed by Van Daele et al., 2014). Five of the event deposits do not show these raised values (e.g., Figure 4b) and are thus not considered in our interpretations. Most probably they contain large amounts of organic matter or volcanic pumice that despite its larger grain size, is relatively light due to its high bubble content. Additionally, one of the sampled intervals contains a crack in the sediments (Figure 4e) and consequently an artificial trough in radiodensity (Figure 3b). The origin of this layer can thus not be stated with certainty but will still be considered together with the remaining events that have not yet been categorized. The remaining 31 event deposits have a significant amount of coarser-grained material, which is either dominant in EM2, EM3, or EM4. In many cases, their coarser-grained content is also reflected in the magnetic properties by the presence of coarser magnetite grains (Figure 3b). The coarsest population, EM4, is related to the granitic grains present in the first pulses of two known seismo-turbidites (SL-F, Figure 4d and SL-D, Figure 4j) that result from onshore landslides (Wils et al., 2018). EM4 is also dominant in another three deposits, all of which contain visually identifiable tephra grains in a muddy matrix (e.g., Figure 4e) and are interpreted as the result of volcanic activity. EM4 is thus not solely composed of turbidites but can more generally be interpreted as containing onshore clastic material.

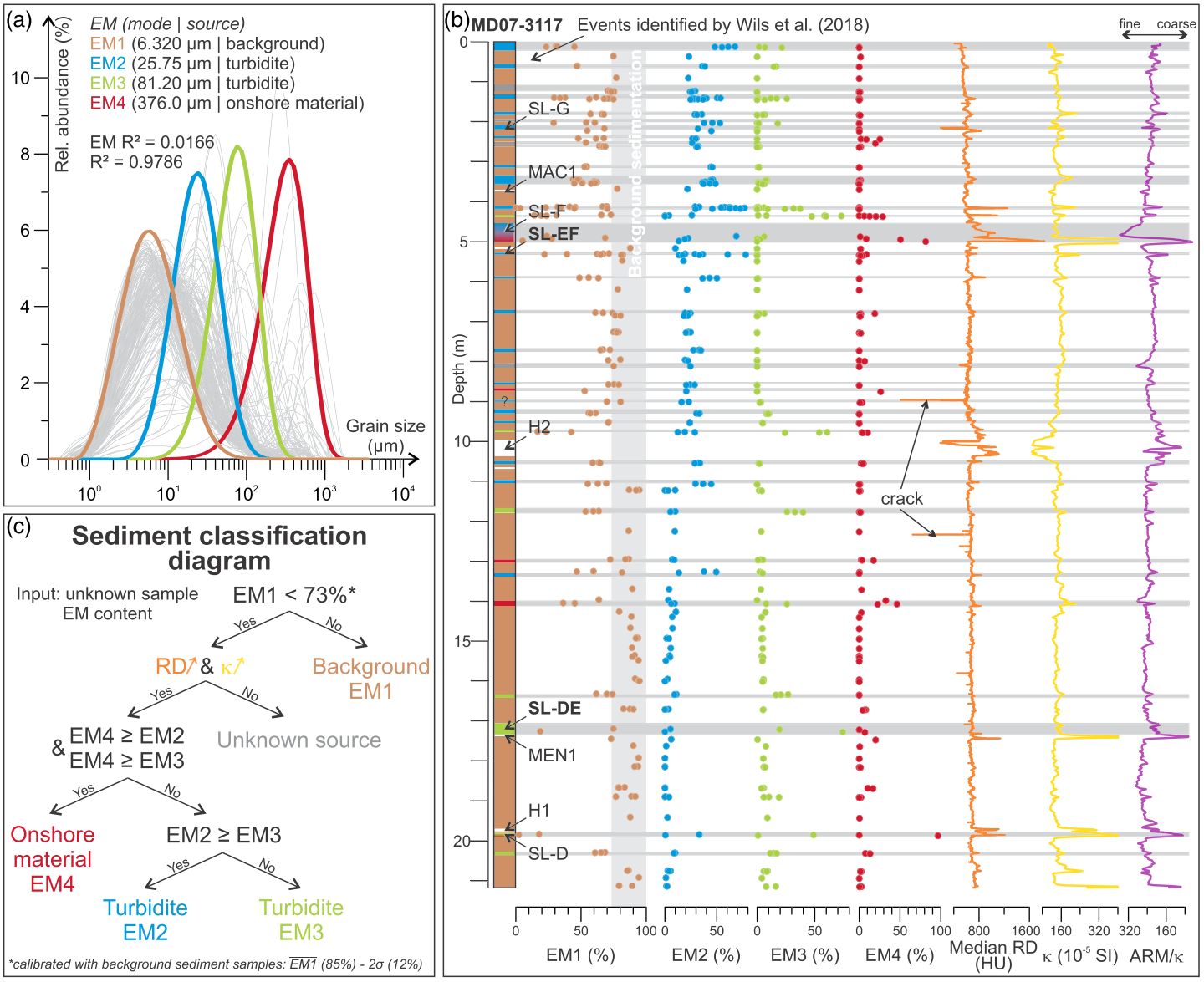

Figure 3. Identification of turbidites in the MD07-3117 sediment core. (a) Grain size results of each of the potential turbidites (gray) is unmixed into four unimodal end-members (EMs)—EM1 (brown, background sedimentation), EM2 (blue, fine-grained turbidite), EM3 (green, coarser-grained turbidite), and EM4 (red, deposition of onshore clastic material). (b) Abundances of each end-member in the different sediment samples, together with the median radiodensity (RD), expressed in Hounsfield Units (HUs) (orange) and some magnetic properties including the volume low-field magnetic susceptibility (κ, yellow, cut off at 400 × 10^{-5} SI for ease of presentation) and an indication of magnetite grain size (ARM/κ, purple). Interpretation of each sediment interval is visualized by a color-coded schematic representation of the sediment core. White layers represent tephra layers that were not analyzed for their grain size. Deposits that were already identified by Wils et al. (2018) are also marked, and those that were interpreted as the result of megathrust earthquakes are indicated in bold. (c) Schematic representation of how each sample is interpreted.

Interpretation of the remaining event deposits (including the nongranitic turbidite pulses of SL-F and SL-D) is based on the relative occurrences of EM2 and EM3. EM3 appears to be dominant in the dark-colored seismo-turbidites SL-DE and SL-D, while EM2 is dominant in SL-G, SL-F, and SL-EF (Figure 4d). These two end-members thus contain earthquake-generated turbidite sedimentation that consists of deltaic material. The other EM2 and EM3 turbidites have similar dark, organic-rich, coarse-grained material (Figures 4 and 5) and can thus also only originate from a delta failure (cf. Van Daele et al., 2014). However, apart from seismically triggered delta collapses, also flood-related hyperpycnal flows and mass-failures, as well as spontaneous failures can occur. The latter is not considered to take place in high-seismicity settings (Praet

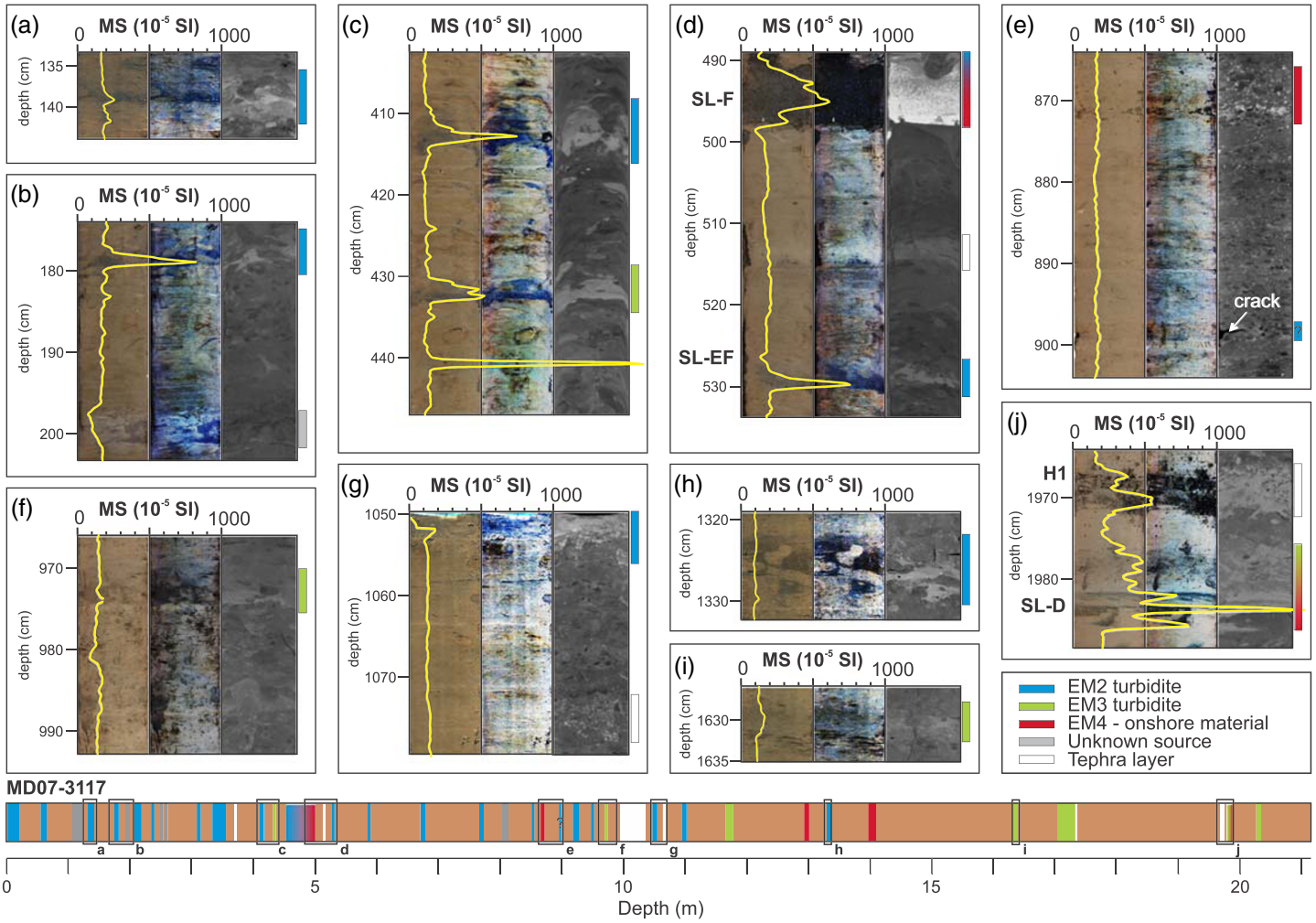

Figure 4. Visualization of selected intervals of the MD07-3117 core. For each interval (a–j, as indicated on a schematic representation of the core), from left to right, a regular RGB-colored, histogram-equalized and CT scan image are presented. Yellow curves represent the magnetic susceptibility (MS) values. All EM2 turbidites are indicated in blue, EM3s in green, EM4 deposits in red, event deposits with an unknown source in gray and tephra/pumice layers in white. Deposits identified by Wils et al. (2018) are also indicated.

et al., 2017) and flood-related deposits in temperate regions are assumed to show higher organic matter content (e.g., Howarth et al., 2014; Simonneau et al., 2013). This would then result in deposits with less pronounced MS and radiodensity peaks like those that have been previously eliminated. Furthermore, flood-related turbidites often show a gradual fining upward trend while the transition from the coarse-grained base to the finer-grained upper part is much sharper for turbidites related to mass movements (Beck, 2009; Vandekerkhove et al., 2019; Wilhelm et al., 2017). As the magnetic properties of MD07-3117 reflect its grain size trend (Figure 3b), the generally strong peak in MS at the base of single-pulse EM2 and EM3 turbidites followed by a rapid decline that can be observed when bioturbation is limited (e.g., Figures 4b–4d) advocates for a nonflood-related triggering mechanism—although this criterion does not rule out the potential occurrence of mass-wasting associated to flooding (e.g., Clare et al., 2016; Vandekerkhove et al., 2019). Given the very high winter precipitation in the area (200–300 mm/month), floods occur on a yearly basis in the Aysén area (Dirección General de Aguas, 2004) but are not reflected in the MD07-3117 core due to the absence of annual or any other type of periodic laminations. Therefore, the remaining EM2 and EM3 turbidites are interpreted as seismo-turbidites, even though flood-triggered mass wasting cannot be completely ruled out. This means that MD07-3117 contains a total of 28 seismo-turbidites of which 21 are EM2-turbidites and 7 are EM3-turbidites

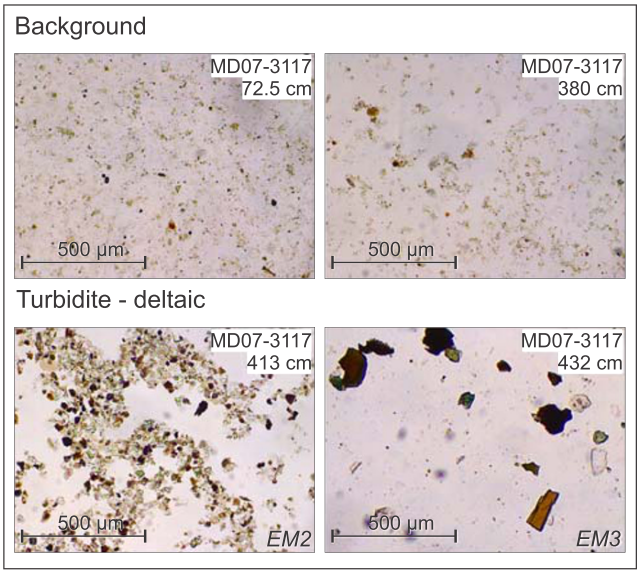

Figure 5. Visualization of smear slides of MD07-3117. Background sedimentation in core MD07-3117 show a mixture of fine-grained minerals with the sporadic occurrence of organic matter and diatoms. The turbidites show much coarser grains and an organic-rich composition (dark-brown to black features), forming typical deltaic facies.

(Figure 3b). A special deposit is the youngest EM3 turbidite (Figure 4c) that apart from deltaic material also contains some granitic grains like those present in the EM4 pulses of turbidites SL-D and SL-F. This implies that some rock slope failures of the fjord walls must have taken place as well. As this turbidite is deposited only shortly after the SL-F turbidite, it might be related to the landslides present directly on top of the MTDs associated to SL-F, as observed by Wils et al. (2018) on seismic profiles (Figure 6).

It is striking that the sandy EM3 turbidites predominantly appear in the lower half of the core and consist of few events, while the silty EM2 turbidites are only present in the upper half and occur much more frequently (Figure 6). Assuming that earthquake recurrence is roughly stable on such a relatively long-time scale, this must be related to a change in turbidite sedimentation dynamics. Seismic profiles in the fjord support this interpretation as high-amplitude reflections start appearing at about 20 ms (two-way travel time, TWT) in the subsurface (~4,400 cal years BP) (Figure 6), which may relate to the abundance of turbidites in the upper 11 m of the core. This relatively sudden appearance of EM2 turbidites can be explained by a gradually prograding delta, allowing an abrupt change in the depositional setting of the core site when the turbidity-current flow path becomes short enough to overcome the distance threshold and to start recording fine-grained turbidites. This flow path distance may have been reduced abruptly, as the prograding delta front reached the two elongated islands to its west (Isla Partida and Isla Carmen; Figure 2) and/or by lateral migration of the river mouth. Indeed, we consider the current EM2-sediment source for the MD07-3117 core site to be the central branch of the Aysén River Delta that is closed in by the two elongated islands. Multibeam bathymetry shows some asymmetrical sediment waves, which were interpreted as upslope migrating bedforms in this channel (Figure 7) similar to those described by Clare et al. (2016) for a fjord head delta in Canada. This points to frequent passing of turbidity currents and thus an active delta section. EM3 turbidites are then interpreted as the result of different but still deltaic, source locations, potentially in combination with (slightly) stronger seismic shaking. The latter induces larger delta collapses that lead to stronger turbidity currents with a higher sediment load (cf. Moernaut et al., 2014), allowing for (coarser grained) sediments to be transported further. This would explain an EM3 source that is located further from the core site, like the northern section of the Aysén River Delta (Figure 2), thus requiring more voluminous delta failures to overcome the distance-related depositional threshold and be recorded in the MD07-3117 core. Also, the Condor River Fan could be a source for EM3 turbidites, located closer to the core location (Figure 2). In this case, the less frequent occurrence of EM3 turbidites shows that the fan is probably less susceptible to failures compared to the EM2 source in the Aysén River Delta, although coarser material can be deposited at the coring site without the prerequisite of a larger delta failure. Regardless of the exact origin of EM3 turbidites, this implies that the shaking intensity threshold for EM3 turbidites is probably slightly higher than for EM2 turbidites. The exact threshold value cannot be determined, but this may well be only just above V½ and almost certainly below VI½ as other types of MTDs are not consistently associated to the EM3 turbidites (Vanneste et al., 2018). This elevated threshold is probably not true for the EM3 turbidite above the H2 deposit (Figure 4f), for which the coarser grain size can be attributed to the H2 volcanic eruption, which deposited a huge amount of (coarse grained) tephra in the fjord (Wils et al., 2018) and its catchment (Naranjo & Stern, 1998), in this way also affecting the fjord's posteruption sedimentation.

Although the actual explanation for the EM3-EM2 transition cannot be determined with certainty, it implies that our record of past earthquakes before ~4,400 cal years BP is incomplete. During the last 4.4 ka, the influence of climate variability on the available turbidite record is assumed to be limited. Precipitation and westerly strength in the region increased significantly around 8 ka and remained high since then (Fiers et al., 2019). Deglaciation in the Aysén Fjord area itself is assumed to have been completed at 15 ka, and glaciers in its catchment probably reached its current state between 10 and 5 ka (Davies et al., 2020). This shows that steady propagation of the Aysén River Delta must have been occurring at least since ~5 ka and probably

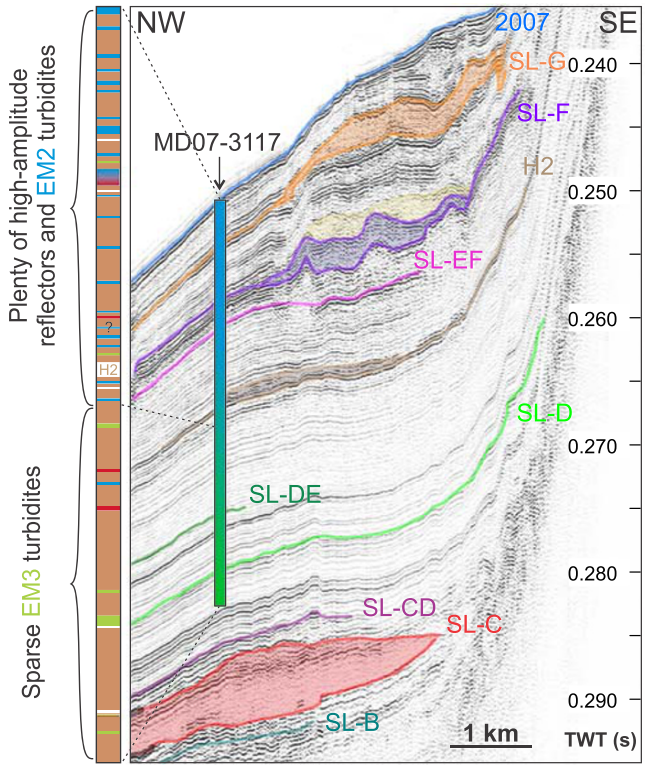

Figure 6. Part of a seismic profile (expressed in two-way travel time, TWT, vertical exaggeration 210 times) that runs over the MD07-3117 core location (see Figure 2 for exact location) with indication of MTDs and stratigraphic levels as identified by Wils et al. (2018). All seismo-turbidites identified by grain size analysis are schematically represented and color-coded according to Figure 3, and the H2 tephra layer is indicated for ease of correlation to the seismic profile. The core can be considered to consist of two facies, where the upper part contains plenty of EM2 turbidites (blue) that seem to explain the more frequent occurrence of high-amplitude seismic reflectors, and the lower part contains only few EM3 turbidites (green). The seismic profile also shows the presence of an additional MTD (yellow) directly on top of those associated to SL-F, which might explain the youngest EM3 turbidite. Figure adapted from Wils et al. (2018).

already sooner. Additionally, after a rapid Early-Holocene sea level rise following deglaciation, relative sea level in southern Chile has shown a relatively stable decline since ~7 ka (Dura et al., 2016; Garrett et al., 2020). Therefore, the time window in which a stable turbidite-based paleoseismic record can be obtained is limited to the last 7,000 years. To extend our current record of ~4,400 years in Aysén to this maximum possible timeframe, a transect of long cores over the migrating turbidite depocenter is required, where the more delta-proximal cores may provide a complete turbidite record for the oldest periods.

4.3. Crustal- Versus Megathrust-Earthquake-Induced Deposits

To identify which of the 28 seismo-turbidites are megathrust-earthquake related, we consider that megathrust earthquakes can produce a seismic intensity of maximum ~VI–VI½ in the Aysén Fjord area (cf. USGS, 2018) due to the large distance (~150 km) to the seismogenic area of the megathrust. This means they can trigger delta failures (threshold V½) but are unable to cause any large-scale onshore rock slope failures (threshold VII½), assuming the intensity thresholds have not changed much over time (Vanneste et al., 2018; Wils et al., 2018). As a consequence, all seismo-turbidites that consist solely of deltaic material and are not associated with onshore landslides, that is, all except SL-G, SL-F, SL-D, and the youngest EM3 turbidite, are considered associated to megathrust earthquakes, bringing the total number of megathrust-earthquake related turbidites to 24. This is in agreement with previous research that already linked events SL-G, SL-F, and SL-D to crustal earthquakes and SL-EF and SL-DE to megathrust earthquakes (Vanneste et al., 2018; Wils et al., 2018). However, it is important to note that some far-field crustal (such as the 1927 earthquake) or intraslab earthquakes may have a similar effect in terms of seismic shaking on the fjord as megathrust earthquakes, resulting in the same turbidite signal in the sediment core. A possibility is that the youngest EM3 turbidite might be an expression of such intraplate earthquake, triggering failure of a granitic slope outside the fjord as well as a delta in the fjord. In any case, the recurrence interval of crustal earthquakes causing MTDs in Aysén Fjord (average interval: ~2,100; shortest interval: ~800 years; Wils et al. (2018)) is about 1 order of magnitude larger than the high-frequency interval with which megathrust earthquakes strike (280 or 140 years, respectively for $M_w \geq 8.6$ or $M_w \geq 7.7$; Moernaut et al., 2018). Additionally, using the intensity prediction equation of Bakun and Wentworth (1997), which is considered to provide good estimates of shaking intensities in Aysén Fjord (Vanneste et al., 2018), only those M_w 7.0 crustal earthquakes with an epicenter in a range of ~100 km from Aysén Fjord are able to cause shaking intensities of V½ or higher. This means that an earthquake like the one in 1927 occurring just over 100 km from the fjord will probably not be able to cause sufficient shaking in the fjord to trigger a delta failure. Additionally, M_w 7.0 crustal earthquakes that occur within ~50 km from the fjord cause shaking intensities of VI½ or higher, meaning that other types of MTDs would start appearing as well (Vanneste et al., 2018). For M_w 6.0, the zone in which earthquakes can only trigger delta failures becomes even smaller, ~20 to 45 km. In other words, the range in which crustal earthquakes can potentially trigger delta failures and thus turbidity currents without the appearance of MTDs in the fjord is rather limited. Furthermore, a recent study has shown that, independent of the seismic intensity, the low-frequency content of interplate-earthquake shaking compared to intraplate-earthquake shaking results in preferential failure of (offshore) soft sediments, as opposed to onshore rocks (Van Daele, Araya-Cornejo, et al., 2019). Hence, LOFZ earthquakes likely have a lower probability of triggering delta failures then megathrust earthquakes, even when causing the same seismic intensities. In combination with their low recurrence rates, it is fair to assume that only exceptionally an event might be erroneously

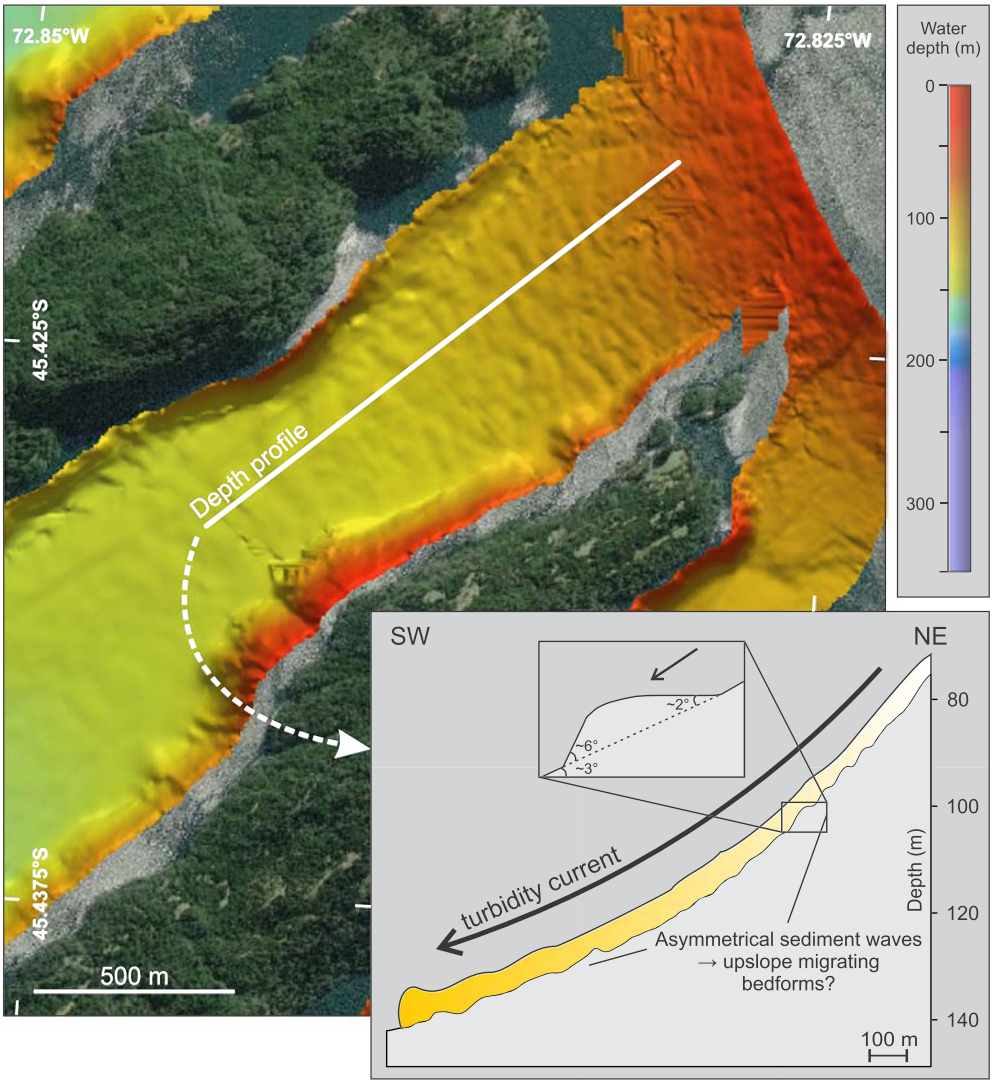

Figure 7. Multibeam bathymetry of one of the channels of the Aysén River Delta (see Figure 2 for location) where some clear asymmetrical sediment waves (zoom showing their slope angles), interpreted as upslope migrating bedforms, can be observed and point to the presence of turbidity flows. A depth profile (vertical exaggeration 14 times) over these structures is presented as an inset.

attributed to megathrust earthquakes because a crustal earthquake as triggering mechanism cannot be completely ruled out.

4.4. A Revised Age-Depth Model

As most of the potential megathrust-earthquake related turbidites are present in the upper part of the core and many of the event deposits identified in Figure 3b were not considered in the age-depth model defined by Wils et al. (2018), the latter was refined by additional radiocarbon dates in the upper part (Table S3) as well as by considering all event deposits in the core as instantaneous. The updated model (Figure 8) shows a rather constant event-free accumulation rate of about 2.0 mm/year, with only some minor deviations from the original model that showed an overall average background sedimentation rate of 2.2 mm/year. This difference can be attributed to the fact that the amount and thickness of event deposits has been updated. This update shows that some of the samples measured by Wils et al. (2018) were effectively retrieved in an event deposit and might thus be reworked, explaining their apparent too old age. Some other outliers in the age-depth model originate from the small samples for which preparation and measurement poses

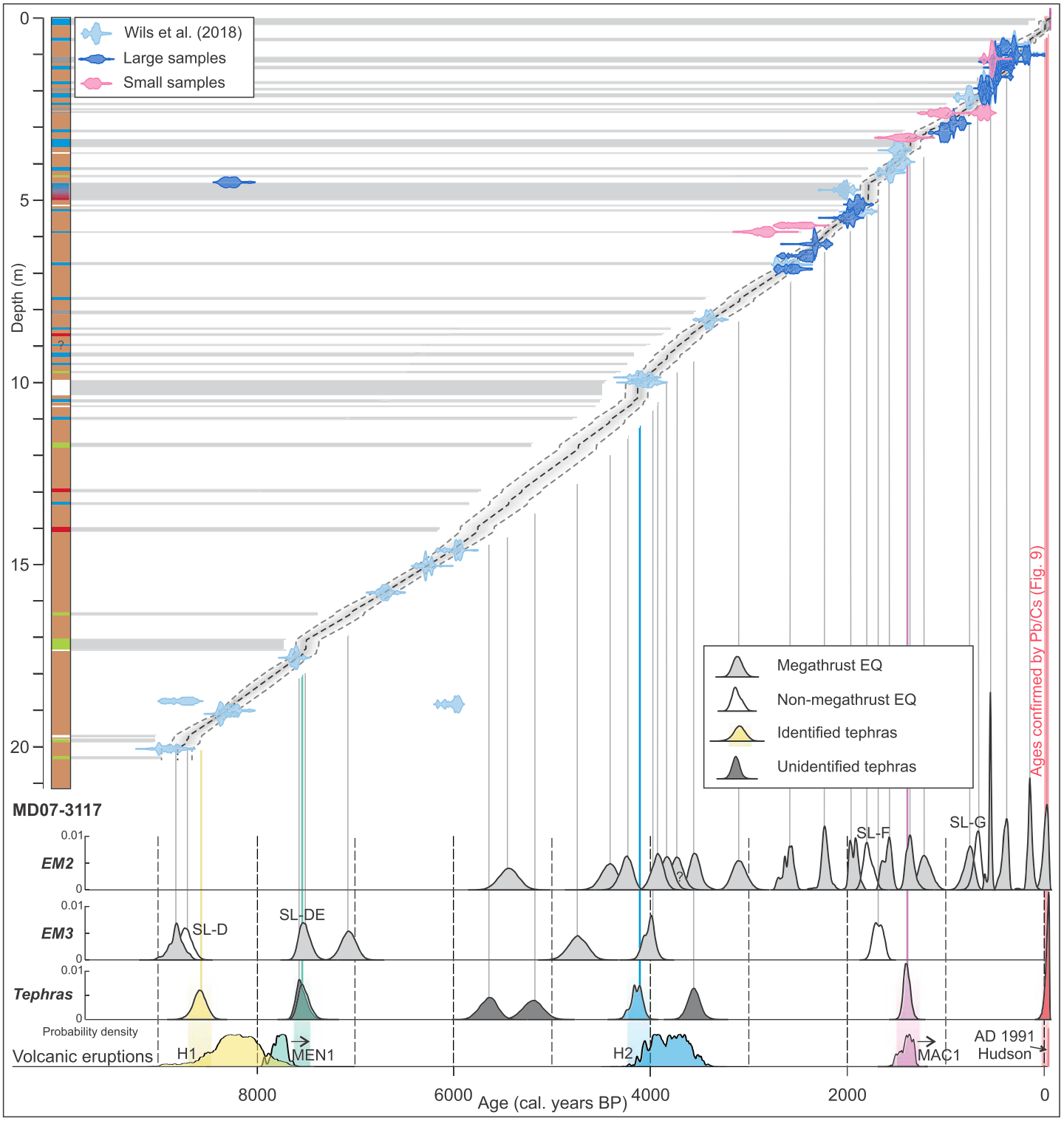

Figure 8. Radiocarbon-based age-depth model of MD07-3117 (95% confidence interval with mean age indicated by black dashed line) showing the age distributions for all tephras and seismo-turbidites identified in the core. Ages of large individual samples are indicated in shades of blue: those that were already measured by Wils et al. (2018) in light blue, new samples in dark blue. Small samples are indicated in pink. The most recent earthquake (EQ) and tephra ages are confirmed by short-lived radionuclide dating (see Figure 9). Age distributions of major Holocene eruptions (H1, MEN1, H2, MAC1, and the AD 1991 Hudson eruption) dated onshore are indicated on the lowermost age axis (Naranjo & Stern, 1998, 2004; Stern & Weller, 2012) and are correlated to their corresponding deposits in the core (verified by geochemical analysis in Wils et al., 2018, or this research) by color coding. Adapted from Wils et al. (2018).

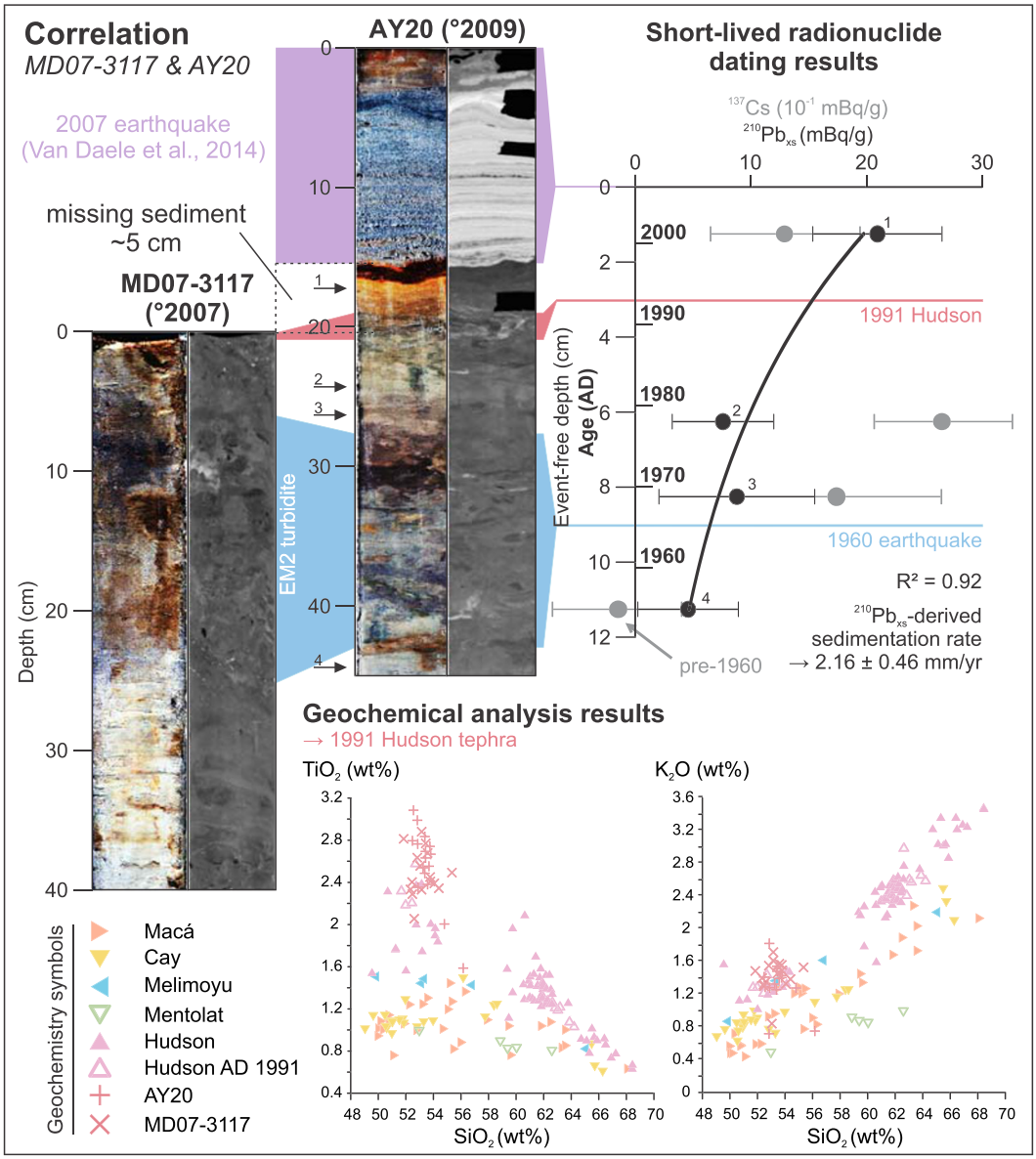

Figure 9. Correlation between the top of MD07-3117 and the short-lived radionuclide-dated AY20 short core (histogram-equalized and CT scan image) based on geochemical analysis of a tephra layer (red) in both cores. The geochemical composition of this tephra, expressed here by TiO_2 and K_2O versus SiO_2 plots, is presented in the bottom part of the figure, together with data for tephra deposits of nearby volcanoes Macá, Cay, Melimoyu, Mentolat, and Hudson (D'Orazio et al., 2003; Gutiérrez et al., 2005; Haberle & Lumley, 1998; Kratzmann et al., 2009; Naranjo & Stern, 1998, 2004). The Pb-based age model of AY20 using event-free depths and the 2007 turbidite (purple; Van Daele et al., 2014) as top is presented, together with the amount of ^{137}Cs that can be detected in each sample (1 to 4, sampling depths indicated by arrows). These results allow to confirm Hudson's AD 1991 eruption as tephra source and the 1960 Great Chilean earthquake as responsible for the youngest EM2 turbidite (blue).

enhanced difficulties (Delqué-Količ et al., 2013). This explains why their results are not always in line with the vast majority of radiocarbon ages that consistently plot within the 95% confidence interval of the obtained model. Moreover, the ages of geochemically identified tephra deposits in the MD07-3117 core (Wils et al., 2018) match those provided in literature (Figure 8). The obtained chronology can thus be considered reliable.

Because detailed correlation to the AY20 short core shows that the upper 5 cm of the MD07-3117 core was lost (Figure 9), all sample depths are corrected by adding 5 cm to construct the age model. Correlation is achieved by a tephra layer that clearly has the same origin in both cores, as shown by their identical

brown to transparent glass shards and their geochemical basaltic trachyandesite composition. Considering the high TiO_2 and K_2O content, these tephra grains can be related to the less evolved products of the Hudson Volcano (D'Orazio et al., 2003; Gutiérrez et al., 2005; Haberle & Lumley, 1998; Kratzmann et al., 2009; Naranjo & Stern, 1998, 2004). Consequently, the uppermost EM2 turbidite in MD07-3117 can also be correlated to the oldest turbidite in AY20. The radiocarbon-based age model shows that this turbidite as well as the Hudson tephra must have been deposited during historical times, and thus, we dated these based on short-lived radionuclides (Figure 9).

Based on the exponential decrease in $^{210}Pb_{xs}$ with depth, a mean sedimentation rate of 2.16 ± 0.46 mm/year was inferred using the Constant Flux Constant Sedimentation model (Oldfield & Appleby, 1984). This matches the overall sedimentation rate for core MD07-3117. Taking into account the 2007 age of the turbidite at the top of AY20, the tephra layer would thus have been deposited in 1989–1995 and the correlated turbidite in 1954–1972. This means that the tephra deposit can be attributed to the Hudson AD 1991 eruption and the 1960 Great Chilean earthquake can be considered responsible for the most recent megathrust-earthquake related turbidite. As the detected amounts of ^{137}Cs are very low (<3 mBq/g) with large 1σ errors bars (up to 0.9 mBq/g), the peak of maximum fallout cannot be confidently identified. Therefore, the only reasonable information provided by this artificial radionuclide is the fact that it is only detected above what we consider as the 1960 turbidite. As ^{137}Cs was first detected in the environment in 1954 and is most prominent in the mid-1960s (Pennington et al., 1973), this also confirms our interpretation (Figure 9).

5. Discussion

5.1. Grain Size Analysis as Tool for Turbidite Paleoseismology

End-member analysis of grain size data on a sediment core from Aysén Fjord has allowed to distinguish different types of turbidites from background sedimentation. This provides a quantitative, objective, and user-independent methodology for turbidite identification and classification, especially when bioturbation is important, significantly improving the rather subjective visual distinctions that have previously been used (e.g., Patton et al., 2015; Pouderoux et al., 2012; St-Onge et al., 2004; Van Daele, Araya-Cornejo, et al., 2019). Because of the strong compositional differences of deltaic material compared to the surrounding fjord walls, the source of each turbidite type was determined. Moreover, thorough knowledge on the sedimentary dynamics in the fjord obtained from the study of seismic reflection profiles (Van Daele et al., 2013; Wils et al., 2018) in combination with several short cores (Van Daele et al., 2014) aided in the identification of a seismic origin for most of the identified turbidites and the exclusion of other potential triggers such as floods and spontaneous failures. To apply this grain size-based paleoseismic methodology to other marine or lacustrine settings around the world, it is thus crucial to understand the different possible source locations for turbidity currents as well as the mechanisms that can generate them.

In complex seismo-tectonic settings where different types of earthquakes can occur, information on the type of earthquake that generated each type of turbidite can be gained by taking into account the levels of seismic shaking that are required to trigger failures in different source areas. These intensity thresholds are site-specific and are crucial to confidently distinguish intraplate from interplate earthquakes. However, depending on the distance between the studied location and the rupture area of each earthquake, differentiating between both types can be challenging and often requires complementary data. Correlations to other available paleoseismic records in the same region can validate the interpretations because strong crustal earthquakes (M_w ~ 6–7) have much smaller rupture areas than strong megathrust earthquakes (M_w ~ 8–9). Moreover, ground motion from strong crustal earthquakes decreases much more rapidly with distance, as can be seen when comparing ground-motion attenuation formula for both earthquake types (Bakun & Wentworth, 1997, and Barrientos, 1980, respectively). In some specific cases, ground motion frequency spectra of each earthquake type can provide a solution as instability of rock slopes may preferentially occur during higher-frequency ground motion typical for shallow crustal earthquakes, whereas the low-frequency ground motion from (more distant) megathrust events has a larger impact on subaqueous sediment slopes (Van Daele, Araya-Cornejo, et al., 2019).

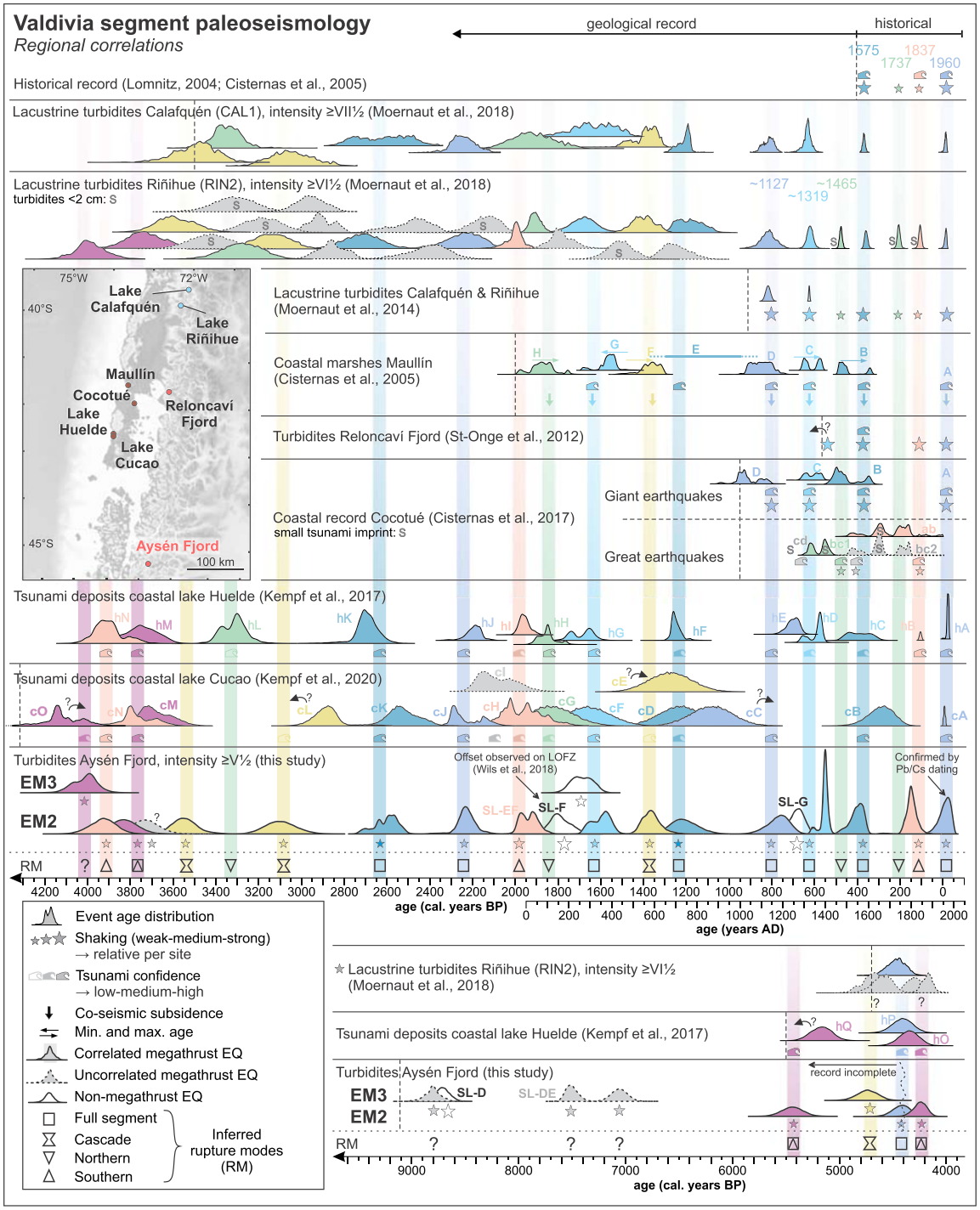

Figure 10. Age correlation of turbidites in Aysén Fjord with different types of megathrust earthquake (EQ) evidence (see legend) observed in several localities along the Valdivia segment. As there are several coastal records available, only a representative selection (i.e., containing all known events) is presented in this overview: Maullín (Cisternas et al., 2005), Cocotué (Cisternas, Garrett, et al., 2017), Lake Huelde (Kempf et al., 2017), and Lake Cucao (Kempf et al., 2020). Additionally, the lacustrine records of Calafquén and Riñihue (Moernaut et al., 2014, 2018) and the only other fjord record available (Reloncaví; St-Onge et al., 2012) are shown. Dashed vertical lines indicate the oldest sediments in each of the presented records. Color coding and upward fading beams of equal and arbitrary width illustrate the suggested correlations that become more tentative toward the northern paleoseismic sites, especially for events older than 2,000 cal years BP. These correlations allow to infer the most likely rupture modes (RMs; see also Figure 11), with decreasing confidence levels toward the older events: Full ruptures are presented in shades of blue, northern ruptures in green, southern in pink, and rupture cascades in yellow. When different rupture modes are possible to explain the available evidence, purple shading is applied. Note the difference in scaling for the last 4,300 cal years BP (upper part) and the first part of the Holocene (lower part). Figure adapted from Moernaut et al. (2018).

5.2. The Aysén Record and Regional Correlations

The MD07-3117 core in Aysén Fjord contains 24 turbidites that are interpreted as the potential result of megathrust earthquakes during the last 9,000 years, of which 21 occurred in the last 5,500 years. We compare their age distributions to the ages of megathrust earthquakes identified by correlation between different paleoseismic sites along the Valdivia segment (Cisternas, Garrett, et al., 2017; Cisternas et al., 2005; Kempf et al., 2020, 2017; Moernaut et al., 2014, 2018; St-Onge et al., 2012) (Figure 10). When the age range of a turbidite in Aysén Fjord overlaps with the age range of a known event—taking into account geological and stratigraphic plausibility—the previously established correlation (Moernaut et al., 2018) can thus be extended to the south. However, these correlations are tentative considering the large distance between the northernmost records and Aysén Fjord, especially for events older than the records in the central third of the Valdivia segment (>2,000 cal years BP; Figure 10). Moreover, event ages obtained in different paleoseismic sites are based on different approaches (i.e., continuous age-depth models in subaqueous records and bracketing of events with minimum/maximum ages for onshore records) and are of variable quality, making them difficult to compare. Therefore, a full review of existing dating information that standardizes the approach to generating event chronology is needed. This would allow application of a statistical test for synchronicity, significantly improving the current technique of visual distribution matching.

Regional correlation of paleoearthquake records shows that several events do not have a counterpart in Aysén Fjord, but all expect one of the potential megathrust-earthquake related events <5,500 cal years BP in Aysén Fjord do correspond to one of the previously identified events. This validates our hypothesis that the vast majority—if not all—of seismo-turbidites in Aysén Fjord that are not associated to MTDs can be considered as generated by megathrust earthquakes. Additionally, none of the seismo-turbidites could be matched with the AD 1927 magnitude 7.1 crustal earthquake, demonstrating that far-field crustal earthquakes indeed have a limited distance range in which they are capable of triggering delta failures in the fjord. The only potentially megathrust-generated seismo-turbidite that cannot be matched to other events along the Valdivia segment is the one around 3,750 cal years BP. This must thus be the result of a small, single-asperity megathrust or far-field intraplate earthquake, or it was erroneously considered as seismically generated due to a crack in the core that does not allow to infer its correct radiodensity (Figures 3b and 4e). The oldest previously identified event on the Valdivia segment is a tsunami deposit in Lake Huelde that slightly overlaps in age with the oldest EM2 turbidite in Aysén Fjord (~5,500 cal years BP). All older events in Aysén Fjord form the oldest documented megathrust earthquakes on the Valdivia segment up to now, although for these events, other long paleoseismic records on the Valdivia segment and more detailed knowledge on crustal earthquakes on the LOFZ (e.g., maximum magnitude and rupture length, recurrence intervals, active fault sections, sedimentological imprint) are required to verify their megathrust-related origin. In any case, they represent an incomplete record as only EM3 turbidites were recorded during these times and these probably result from slightly higher shaking intensities in the fjord area compared to EM2 turbidites. Additionally, effects of westerlies, sea level changes and glacier proximity on the sedimentary record need to be considered to determine the significance of events >4,400 cal years BP.

5.3. Implications for Spatial and Temporal Earthquake Recurrence

To reliably identify earthquake rupture modes, we will focus on events that occurred during the last ~2,000 years for which paleoseismic evidence is available in most parts of the Valdivia segment (Figure 11). Events will be referred to by using their age approximation, which is either based on historical data, the mean age in Aysén Fjord or ages obtained at other paleoseismic sites, either to allow for ease of comparison as an age for this event was already specifically mentioned in literature (e.g., the AD ~1319 and ~1127 events) or because the event is not identified in Aysén Fjord (e.g., AD ~100).

Based on the currently available paleoseismic evidence in combination with the newly identified megathrust-earthquake related turbidites in Aysén Fjord, we suggest a rupture model with alternations of three major types of ruptures: full-segment, partial, and cascading ruptures. During full-segment ruptures, the entire length of the Valdivia segment ruptures in a single event, generally with $M_w \geq 9$ (Wells & Coppersmith, 1994). Partial ruptures, on the other hand, are much smaller and rupture only part of the segment. This can be either a single-asperity rupture, generally assumed to be around M_w 7.5–8.5, but also includes multiasperity ruptures that reach even higher magnitudes like during the AD 1837 earthquake (M_w ~ 8.8–9.5; Cisternas, Carvajal, et al., 2017). Both full-segment and partial rupture types are known

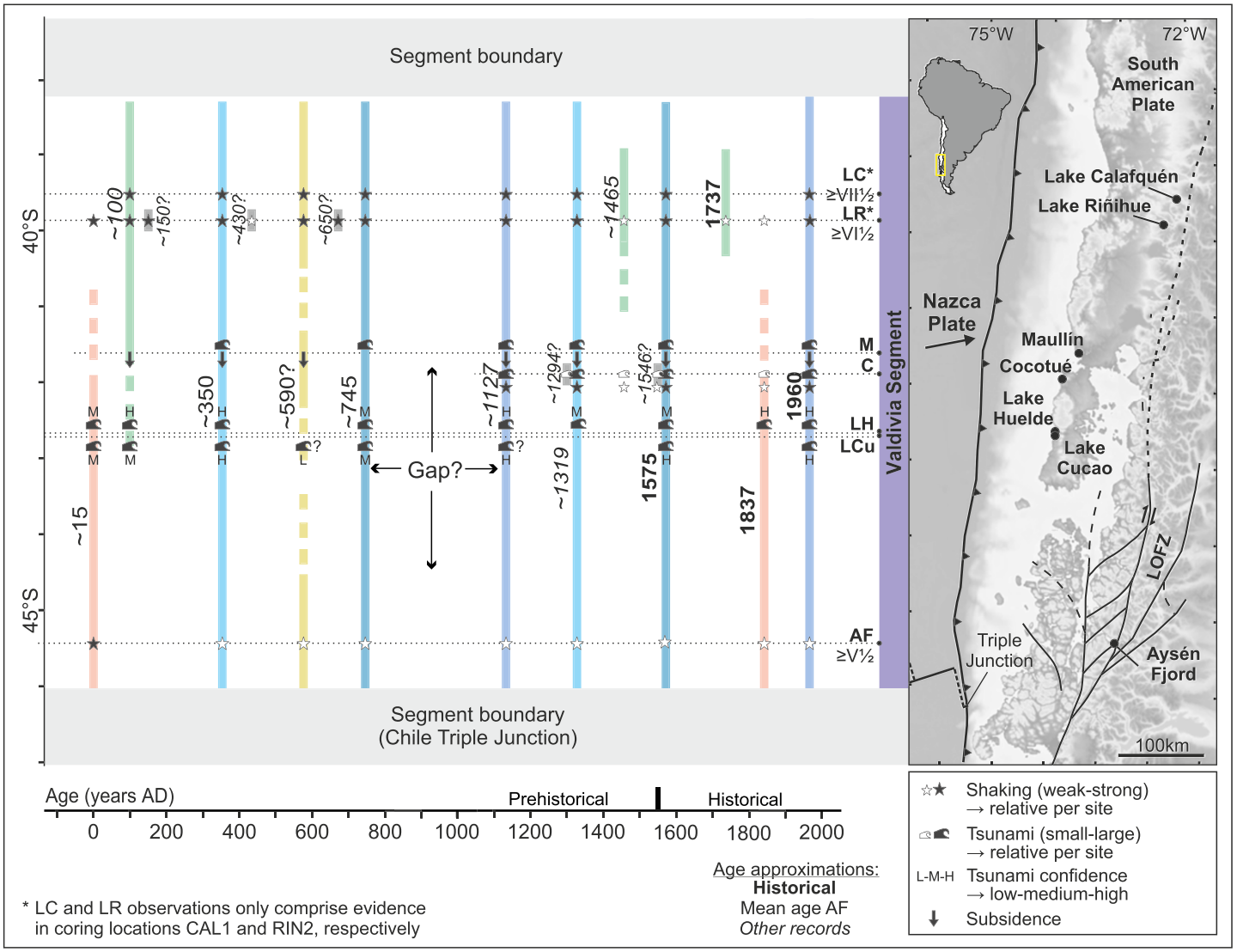

Figure 11. Proposed rupture modes for the last ~2,000 years inferred from paleoseismic evidence in Lake Calafquén (LC; Moernaut et al., 2018), Lake Riñihue (LR; Moernaut et al., 2018), Maullín (M; Cisternas et al., 2005), Cocotué (C; Cisternas, Garrett, et al., 2017), Lake Huelde (LH; Kempf et al., 2017), Lake Cucao (LCu; Kempf et al., 2020), and Aysén Fjord (AF; this study). All observations are presented aligned with the inferred event age (either based on the historical record (bold), the mean age in Aysén Fjord (normal), or an approximation based on other records (italic) for events that have already been described or cannot be identified in Aysén Fjord) and rupture patterns are color coded according to Figure 10. Variable rupture modes exist, with regular 1960-like full ruptures as well as partial ruptures in the northern or southern part of the segment. Prehistorical partial ruptures that do not appear to affect large portions of the Valdivia segment are shown in gray. There is a consistent gap or quiet period between AD ~745 and ~1127, with absence of paleoseismic evidence in all localities.

from historical records of earthquakes along the Valdivia segment (Lomnitz, 2004). Similar alternations of full and partial ruptures have also been inferred along, for example, the Nankai Trough (Garrett et al., 2016) and Japan Trench (Satake, 2015) as well as the Hikurangi Margin in New Zealand (Clark et al., 2019). Cascading ruptures combine several adjacent smaller partial ruptures along the entire length of the segment within a relatively short timeframe (up to years-decades). Up to now, this phenomenon has not been observed along the Valdivia segment but has already been described along the Maule segment of the Chilean subduction zone, just north of the Valdivia segment. There, two $M_w > 8$ earthquakes occurred within 5 years' time (AD 2010 and 2015) on nearby fault sections (Melnick et al., 2017). Similar cascading events have been observed along the Sunda megathrust (Philibosian et al., 2017). Melnick et al. (2017) explain such events by an elastic response of both the oceanic and continental plate to coseismic and post seismic fault slip that results in higher shear stresses and increased locking on adjacent fault sections, in this way increasing the strain accumulation rates and bringing these sections closer to failure.

The last major rupture of the Valdivia segment occurred in 1960, for which evidence can be found in all paleoseismic sites, including Aysén Fjord. This shows that shaking intensities of about V½ must have been achieved in the area, implying that the unverified values of IV given by Lazo Hinrichs (2008) based on newspaper reports are probably an underestimation. Modeled values by USGS (2018) using ground-motion prediction equations and taking into account, for example, rupture area and site effects probably better represent the actual shaking at the time. In the preceding 2,000 years, similar segment-wide paleoseismic evidence can be found at four other timings (AD 1575, ~1319, ~1127, and ~350). This hints toward the occurrence of additional full-segment ruptures, even though shaking intensities of ≥V½ in Aysén Fjord do not necessarily require a rupture extending all the way to the Triple Junction. Ruptures ending farther north would require a significant amount of slip there, that is, at least the amount that occurred during the 1960 earthquake (>20 m; Moreno et al., 2009), to still produce sufficient shaking intensities in Aysén Fjord. With such enormous amount of slip it would, however, be rather unlikely that the rupture does not propagate to the south to produce a full rupture as historical ruptures in AD 1960 and 1837 showed that there are no persistent segment boundaries in the southern part of the Valdivia segment (cf. Cisternas, Carvajal, et al., 2017). Moreover, if ruptures consistently stop farther north, this leaves a slip deficit in the southern part of the Valdivia segment that has not been accommodated as no additional southern ruptures have been registered in Aysén Fjord. This shows the added value of the paleoseismic record in Aysén Fjord, for the first time allowing to confidently state that full-segment ruptures are not uncommon for the Valdivia segment.

A fifth 1960-like combination of paleoseismic evidence can be found around AD ~745, albeit without observations of coseismic subsidence in Maullín (Cisternas et al., 2005). This could be explained by a full rupture during which slip—at the latitude of Maullín—is located only on the deeper part of the megathrust's seismogenic zone so that no subsidence occurred there (cf. Cisternas, Carvajal, et al., 2017). A similar interpretation is invoked to explain observations of coseismic coastal subsidence on the Kamchatka subduction zone (Pinegina et al., 2020). Alternatively, activation of a splay fault could also explain a change in the subsidence and uplift pattern and can release some of the shear stress that is accumulated on the megathrust, in this way possibly contributing to variability in megathrust earthquake behavior as demonstrated by Cummins et al. (2001) for the Nankai Trough. This would be consistent with the absence of any type of paleoseismic evidence between this seemingly unusual event and the full rupture of AD ~1,127. In this way, there is a clear quiet period of about 400 years, which is about twice that of any other interseismic period in the last 2,000 years. This could potentially mark the onset of a supercycle as inferred along the Cascadia Margin, where event clusters alternate with large gaps (Goldfinger et al., 2013).

This compilation allows us to advocate for the occurrence of six full ruptures of the Valdivia segment during the last 2,000 years, including the 1960 earthquake, with a recurrence interval of 321 ± 116 years (1σ of the interval times) when using the mean ages for each event as provided by the age-depth model in Aysén Fjord. This is somewhat longer than formerly assumed as the record in Aysén shows that some of the previously considered 1960-like ruptures (e.g., AD ~100) should be reinterpreted. It shows that the M_w 9.51960 earthquake was not unique for the region and similarly catastrophic events might thus reoccur in future times. These are not only capable of causing significant shaking-related damage over >1,000 km along-strike; they can also trigger trans-Pacific tsunamis with far-field damage potential, as was the case for the tsunami following the 1960 Great Chilean Earthquake (Lomnitz, 2004), killing hundreds of people in places as far as Japan (Lazo Hinrichs, 2008). This implies a significant hazard not only for south-central Chile but also for other countries across the Pacific.

Partial ruptures include the historical 1737 and 1837 events, respectively, in the northern and southern part of the Valdivia segment. A prehistoric counterpart for the 1837 earthquake occurred in AD ~15. This event was potentially even larger, considering the presence of small MTDs in Aysén Fjord (SL-EF; Wils et al., 2018) as a result of higher shaking intensities (≥VI½, <VIII) in the area (cf. Vanneste et al., 2018). The following event occurred in AD ~100 and appears to have only ruptured the northern third of the Valdivia segment, which is easy to understand considering that the slip deficit in the southern part was probably largely released by the AD ~15 earthquake. This combination of a northern and southern rupture allowed for a period of ~600 years without the occurrence of any full ruptures, which corresponds to almost two complete full-rupture seismic cycles. Partial ruptures can thus accommodate for a significant portion of the stress built-up along the Valdivia segment, in this way postponing the occurrence of full-segment ruptures. A similar phenomenon probably occurred due to the AD 1737 and 1837 events that precede the 1960 earthquake.

Nevertheless, northern and southern partial ruptures do not always occur consecutively (e.g., AD ~1465 and most of the local, single-asperity events). This makes their recurrence highly variable and much less periodic, as was also found by Moernaut et al. (2018). It is also clear that partial ruptures affecting large portions of the megathrust are mostly tsunamigenic. They can even trigger long-distance tsunamis, as is evidenced by tsunami damage in Hawaii and Japan after the AD 1837 earthquake (Lomnitz, 2004). This shows that the Valdivia segment poses a significant seismic and tsunami hazard, even if a full rupture does not occur.

A new rupture mode for the Valdivia segment is invoked to explain the paleoseismic evidence observed at AD ~590. Paleoseismic shaking evidence is recorded along the entire segment, but no conclusive tsunami evidence has been identified up to now: no tsunami deposit has been found in Maullín (Cisternas et al., 2005) or Lake Huelde (Kempf et al., 2017), and the only potential age-matching tsunami deposit in Lake Cucao (cE) has only a minor sedimentary imprint and also low confidence for attributing a tsunami origin (Kempf et al., 2020). Full ruptures unaccompanied by segment-wide tsunamis are unlikely, unless this was a full-segment rupture with mostly a deeper slip distribution that did not rupture the updip parts of the seismogenic zone (cf. AD 1943 earthquake in central Chile; Melgar et al., 2016). However, the downdip limit of the megathrust is usually strongly segmented and patchy (cf. Lay et al., 2012), making it unlikely for a rupture to propagate over ~1,000 km without involving the central (and shallow) part of the megathrust. This AD ~590 event is therefore interpreted as a rupture cascade consisting of several partial ruptures during which different asperities of the Valdivia segment failed within a short time interval. Such partial ruptures may have produced a minor local tsunami and a small tsunami deposit in Lake Cucao. Nevertheless, only the detection of a turbidite stack (cf. Van Daele et al., 2017) comprising two individual turbidites separated by limited amounts of hemipelagic sedimentation near the area between the cascading ruptures could conclusively rule out other rupture scenarios.

The proposed rupture model for the last two millennia shows that full ruptures form the dominant mode, occurring more frequently than partial ruptures at any given location. Intervals between successive full ruptures of the Valdivia segment (~320 years) are relatively short compared to those observed along the Japan trench (~700 years) where they mark the onset of a supercycle during which smaller events (M_w ~ 7.5) take place once every ~37 years (Satake, 2015). This implies that megathrust earthquakes in general occur more frequently along the Japan Trench, but the highest magnitude events are more rare. For the Valdivia segment, similar rupture modes as those inferred for the last two millennia can be invoked to explain the variability of observations prior to 2,000 cal years BP (Figure 10). However, many uncertainties remain due to the lack of paleoseismic evidence in the central third of the Valdivia segment for this period, making it highly speculative to assign a specific rupture mode to any of the current observations. In any case, the Aysén record in combination with other paleoseismic sites shows that the rupture mode of the Valdivia segment is very variable over time. Additionally, the rupture mode of a specific event does not necessarily comply with the preceding rupture mode and is thus not following the simple concepts of the elastic rebound theory in which each rupture resets the stress level to zero. For example, a logical combination of a southern and northern partial rupture occurred in AD ~15 and ~100, while the AD ~1,465 northern partial rupture was followed by a full-segment rupture. This shows that long-term fault memory can be an important factor influencing the occurrence probability and rupture mode of the next earthquake (Salditch et al., 2020) and underscores the need for long paleoseismic records that reconstruct rupture variability in space and time.

6. Conclusions

1. End-member analysis of grain size data of sediment core MD07-3117 in combination with careful consideration of sediment sources has made it possible to distinguish different types of turbidites and reveal those that have been seismically generated.
2. Consideration of the shaking intensities required to trigger the seismo-turbidites in Aysén Fjord allowed to establish the first record of past megathrust earthquakes in the southern third of the Valdivia segment. The record is assumed complete over the last 4,400 years, and three additional events dating back up to ~9,000 cal years BP are found. This extends the current regional paleoseismological record by about 3,500 years.
3. Correlation of these seismo-turbidites to other paleoseismic sites reveals a complex temporal pattern of different rupture modes, focusing on the last 2,000 years. This includes an alternation of 1960-like full-

segment ruptures, cascading ruptures and partial ruptures, the latter comprising both multiasperity and single-asperity ruptures.

4. The occurrence of prehistoric 1960-like ruptures is substantiated for the first time, with an average recurrence interval of ~321 ± 116 years (standard deviation of interval variability) for the last two millennia. This rate varies significantly due to the less frequent and less periodic occurrence of partial or cascading ruptures. For example, a spatial sequence of a southern and northern partial rupture in AD ~15 and ~100, respectively, may have postponed the subsequent full-segment rupture by almost an entire full-rupture seismic cycle.
5. A period of seismic quiescence, where no paleoseismic evidence can be observed at any of the paleoseismic sites for about 400 years, took place after a full-segment rupture that shows an unusual subsidence/uplift pattern in AD ~745.
6. Full ruptures seem to be the most common rupture mode in the last 2,000 years, but intervening smaller events and a quiet period mark a strong variability in the reconstructed rupture mode scenario. Paleoseismic records along the Valdivia segment may allow to estimate the probability for an earthquake at a specific time interval at a given site but currently do not allow confident statements on the rupture mode of the next earthquake. A better knowledge on long-term fault memory is therefore required. Specifically, this demonstrates the need for long paleoseismic shaking records in the central and southern third of the Valdivia segment to establish a rupture reconstruction for events >2,000 cal years BP and fine-tune the proposed scenarios for the last two millennia.

Data Availability Statement

All data required to reproduce the results presented in this research can be found in the manuscript itself or in the supporting information as well as through the general repository Figshare (10.6084/m9.figshare.12356189). The studied sediment core half is currently stored at the VLIZ core repository in Ostend (Belgium).

Acknowledgments

K. W. is currently funded by a PhD scholarship of the Special Research Fund (BOF) of Ghent University. M. V. D. acknowledges the support of Research Foundation—Flanders (FWO) and J. M. the Austrian Science Fund (FWF): project P30285-N34. G. L. recognizes the support by a Catalan Government Grups de Recerca Consolidats grant (2017 SGR 315), and C. K. acknowledges the financial support from the multiinstitutional program LEFE (project PACHIDERME). We thank Rik Achten for the use of the CT scanner in Ghent University Hospital and the Laboratoire de Mesures Carbone 14 (LMC14) in Saclay (France) for radiocarbon dating with Artemis, in particular Emmanuelle Delqué-Količ who took the time to explain the difficulties in dealing with small samples. IHS Markit Kingdom Suite seismic interpretation software is acknowledged for their educational user license. The authors would like to thank Inka Meyer for sharing her expertise with analysis and interpretation of the grain size data. We also thank Marc De Batist for proofreading an earlier version of this manuscript. Two anonymous reviewers are acknowledged for their detailed and constructive comments that improved an earlier version of this manuscript.

References

Bakun, W., & Wentworth, C. (1997). Estimating earthquake location and magnitude from seismic intensity data. *Bulletin of the Seismological Society of America*, *87*(6), 1502–1521.

Barrientos, S. E. (1980). *Regionalización sísmica de Chile, Memoria para optar al grado de Magister en Ciencias con Mención en Geofisica thesis, Universidad de Chile, Santiago, Chile*.

Beck, C. (2009). Late Quaternary lacustrine paleo-seismic archives in north-western Alps: Examples of earthquake-origin assessment of sedimentary disturbances. *Earth-Science Reviews*, *96*(4), 327–344. https://doi.org/10.1016/j.earscirev.2009.07.005

Blaauw, M., & Christen, J. A. (2011). Flexible paleoclimate age-depth models using an autoregressive gamma process. *Bayesian Analysis*, *6*(3), 457–474. https://doi.org/10.1214/11-ba618

Cifuentes, I. L. (1989). The 1960 Chilean earthquakes. *Journal of Geophysical Research*, *94*(B1), 665–680. https://doi.org/10.1029/JB094iB01p00665

Cisternas, M., Atwater, B. F., Torrejón, F., Sawai, Y., Machuca, G., Lagos, M., et al. (2005). Predecessors of the giant 1960 Chile earthquake. *Nature*, *437*(7057), 404–407. https://doi.org/10.1038/nature03943

Cisternas, M., Carvajal, M., Wesson, R., Ely, L. L., & Gorigoitia, N. (2017). Exploring the historical earthquakes preceding the Giant 1960 Chile earthquake in a time-dependent seismogenic zone. *Bulletin of the Seismological Society of America*, *107*(6), 2664–2675. https://doi.org/10.1785/0120170103

Cisternas, M., Garrett, E., Wesson, R., Dura, T., & Ely, L. L. (2017). Unusual geologic evidence of coeval seismic shaking and tsunamis shows variability in earthquake size and recurrence in the area of the giant 1960 Chile earthquake. *Marine Geology*, *396*, 54–66. https://doi.org/10.1016/j.margeo.2018.01.005

Clare, M. A., Hughes Clarke, J. E., Talling, P. J., Cartigny, M. J. B., & Pratomo, D. G. (2016). Preconditioning and triggering of offshore slope failures and turbidity currents revealed by most detailed monitoring yet at a fjord-head delta. *Earth and Planetary Science Letters*, *450*, 208–220. https://doi.org/10.1016/j.epsl.2016.06.021

Clark, K., Howarth, J., Litchfield, N., Cochran, U., Turnbull, J., Dowling, L., et al. (2019). Geological evidence for past large earthquakes and tsunamis along the Hikurangi subduction margin, New Zealand. *Marine Geology*, *412*, 139–172. https://doi.org/10.1016/j.margeo.2019.03.004

Cummins, P. R., Hori, T., & Kaneda, Y. (2001). Splay fault and megathrust earthquake slip in the Nankai Trough. *Earth, Planets and Space*, *53*(4), 243–248. https://doi.org/10.1186/bf03352381

Davies, B. J., Darvill, C. M., Lovell, H., Bendle, J. M., Dowdeswell, J. A., Fabel, D., et al. (2020). The evolution of the Patagonian Ice Sheet from 35 ka to the present day (PATICE). *Earth-Science Reviews*, *204*, 103152. https://doi.org/10.1016/j.earscirev.2020.103152

Delqué-Količ, E., Comby-Zerbino, C., Ferkane, S., Moreau, C., Dumoulin, J. P., Caffy, I., et al. (2013). Preparing and measuring ultra-small radiocarbon samples with the ARTEMIS AMS facility in Saclay, France. *Nuclear Instruments and Methods in Physics Research Section B: Beam Interactions with Materials and Atoms*, *294*, 189–193. https://doi.org/10.1016/j.nimb.2012.08.048

Dirección General de Aguas (2004). Diagnostico y Clasificacion de los Cursos y Cuerpos de Agua Segun Objectivos de Calidad: Cuenca del Río Aysén, Rep.

D'Orazio, M., Innocenti, F., Manetti, P., Tamponi, M., Tonarini, S., González-Ferrán, O., et al. (2003). The Quaternary calc-alkaline volcanism of the Patagonian Andes close to the Chile triple junction: Geochemistry and petrogenesis of volcanic rocks from the Cay and Maca volcanoes (~45°S, Chile). *Journal of South American Earth Sciences*, *16*(4), 219–242. https://doi.org/10.1016/s0895-9811(03)00063-4

Dura, T., Engelhart, S. E., Vacchi, M., Horton, B. P., Kopp, R. E., Peltier, W. R., & Bradley, S. (2016). The role of Holocene relative sea-level change in preserving records of subduction zone earthquakes. *Current Climate Change Reports*, *2*(3), 86–100. https://doi.org/10.1007/s40641-016-0041-y

Ely, L. L., Cisternas, M., Wesson, R. L., & Dura, T. (2014). Five centuries of tsunamis and land-level changes in the overlapping rupture area of the 1960 and 2010 Chilean earthquakes. *Geology*, *42*(11), 995–998. https://doi.org/10.1130/g35830.1

Fiers, G., Bertrand, S., Van Daele, M., Granon, E., Reid, B., Vandoorne, W., & De Batist, M. (2019). Hydroclimate variability of northern Chilean Patagonia during the last 20 kyr inferred from the bulk organic geochemistry of Lago Castor sediments (45°S). *Quaternary Science Reviews*, *204*, 105–118. https://doi.org/10.1016/j.quascirev.2018.11.015

Garrett, E., Fujiwara, O., Garrett, P., Heyvaert, V. M. A., Shishikura, M., Yokoyama, Y., et al. (2016). A systematic review of geological evidence for Holocene earthquakes and tsunamis along the Nankai-Suruga trough, Japan. *Earth-Science Reviews*, *159*, 337–357. https://doi.org/10.1016/j.earscirev.2016.06.011

Garrett, E., Melnick, D., Dura, T., Cisternas, M., Ely, L. L., Wesson, R. L., et al. (2020). Holocene relative sea-level change along the tectonically active Chilean coast. *Quaternary Science Reviews*, *236*, 106281. https://doi.org/10.1016/j.quascirev.2020.106281

Garrett, E., Shennan, I., Woodroffe, S. A., Cisternas, M., Hocking, E. P., & Gulliver, P. (2015). Reconstructing paleoseismic deformation, 2: 1000 years of great earthquakes at Chucalén, south central Chile. *Quaternary Science Reviews*, *113*, 112–122. https://doi.org/10.1016/j.quascirev.2014.10.010

Geersen, J., Völker, D., Behrmann, J. H., Kläschen, D., Weinrebe, W., Krastel, S., & Reichert, C. (2013). Seismic rupture during the 1960 Great Chile and the 2010 Maule earthquakes limited by a giant Pleistocene submarine slope failure. *Terra Nova*, *25*(6), 472–477. https://doi.org/10.1111/ter.12060

Goldfinger, C., Ikeda, Y., Yeats, R. S., & Ren, J. (2013). Superquakes and supercycles. *Seismological Research Letters*, *84*(1), 24–32. https://doi.org/10.1785/0220110135

Goldfinger, C., Nelson, C. H., & Johnson, J. E. (2003). Holocene earthquake records from the Cascadia subduction zone and northern San Andreas fault based on precise dating of offshore turbidites. *Annual Review of Earth and Planetary Sciences*, *31*(1), 555–577. https://doi.org/10.1146/annurev.earth.31.100901.141246

Gutiérrez, F., Gioncada, A., González Ferran, O., Lahsen, A., & Mazzuoli, R. (2005). The Hudson Volcano and surrounding monogenetic centres (Chilean Patagonia): An example of volcanism associated with ridge–trench collision environment. *Journal of Volcanology and Geothermal Research*, *145*(3–4), 207–233. https://doi.org/10.1016/j.jvolgeores.2005.01.014

Haberle, S. G., & Lumley, S. H. (1998). Age and origin of tephras recorded in postglacial lake sediments to the west of the southern Andes, 44°S to 47°S. *Journal of Volcanology and Geothermal Research*, *84*(3–4), 239–256. https://doi.org/10.1016/S0377-0273(98)00037-7

Hogg, A. G., Hua, Q., Blackwell, P. G., Niu, M., Buck, C. E., Guilderson, T. P., et al. (2013). SHCal13 Southern Hemisphere calibration, 0–50,000 years cal BP. *Radiocarbon*, *55*(4), 1889–1903. https://doi.org/10.2458/azu_js_rc.55.16783

Howarth, J. D., Fitzsimons, S. J., Norris, R. J., & Jacobsen, G. E. (2014). Lake sediments record high intensity shaking that provides insight into the location and rupture length of large earthquakes on the Alpine Fault, New Zealand. *Earth and Planetary Science Letters*, *403*, 340–351. https://doi.org/10.1016/j.epsl.2014.07.008

Kempf, P., Moernaut, J., & Batist, M. D. (2019). Bimodal recurrence pattern of tsunamis in south-central Chile: A statistical exploration of paleotsunami data. *Seismological Research Letters*, *90*(1), 194–202. https://doi.org/10.1785/0220180204

Kempf, P., Moernaut, J., Van Daele, M., Pino, M., Urrutia, R., & De Batist, M. (2020). Paleotsunami record of the past 4300 years in the complex coastal lake system of Lake Cucao, Chiloé Island, south central Chile. *Sedimentary Geology*, *401*, 105644. https://doi.org/10.1016/j.sedgeo.2020.105644

Kempf, P., Moernaut, J., Van Daele, M., Vandoorne, W., Pino, M., Urrutia, R., & De Batist, M. (2017). Coastal lake sediments reveal 5500 years of tsunami history in south central Chile. *Quaternary Science Reviews*, *161*, 99–116. https://doi.org/10.1016/j.quascirev.2017.02.018

Komatsubara, J., & Fujiwara, O. (2007). Overview of Holocene tsunami deposits along the Nankai, Suruga, and Sagami Troughs, southwest Japan. *Pure and Applied Geophysics*, *164*(2–3), 493–507. https://doi.org/10.1007/s00024-007-0179-y

Kratzmann, D. J., Carey, S., Scasso, R., & Naranjo, J.-A. (2009). Compositional variations and magma mixing in the 1991 eruptions of Hudson volcano, Chile. *Bulletin of Volcanology*, *71*(4), 419–439. https://doi.org/10.1007/s00445-008-0234-x

Kuehl, S. A., Miller, E. J., Marshall, N. R., & Dellapenna, T. M. (2017). Recent paleoseismicity record in Prince William Sound, Alaska, USA. *Geo-Marine Letters*, *37*(6), 527–536. https://doi.org/10.1007/s00367-017-0505-7

Lastras, G., Amblas, D., Calafat, A. M., Canals, M., Frigola, J., Hermanns, R. L., et al. (2013). Landslides cause tsunami waves: Insights from Aysén fjord, Chile. *Eos*, *94*(34), 297–298. https://doi.org/10.1002/2013EO340002

Lay, T., Kanamori, H., Ammon, C. J., Koper, K. D., Hutko, A. R., Ye, L., et al. (2012). Depth-varying rupture properties of subduction zone megathrust faults. *Journal of Geophysical Research*, *117*, B04311. https://doi.org/10.1029/2011JB009133

Lazo Hinrichs, R. G. (2008). Estudio de los daños de los terremotos del 21 y 22 de mayo de 1960, Memoria para optar al título de Igeniero Civil thesis, 427 pp, Universidad de Chile, Santiago, Chile.

Lomnitz, C. (2004). Major earthquakes of Chile: A historical survey, 1535–1960. *Seismological Research Letters*, *75*(3), 368–378. https://doi.org/10.1785/gssrl.75.3.368

Melgar, D., Fan, W., Riquelme, S., Geng, J., Liang, C., Fuentes, M., et al. (2016). Slip segmentation and slow rupture to the trench during the 2015, Mw8.3 Illapel, Chile earthquake. *Geophysical Research Letters*, *43*, 961–966. https://doi.org/10.1002/2015GL067369

Melgar, D., Riquelme, S., Xu, X., Baez, J. C., Geng, J., & Moreno, M. (2017). The first since 1960: A large event in the Valdivia segment of the Chilean Subduction Zone, the 2016 M7.6 Melinka earthquake. *Earth and Planetary Science Letters*, *474*, 68–75. https://doi.org/10.1016/j.epsl.2017.06.026

Melnick, D., Bookhagen, B., Strecker, M. R., & Echtler, H. P. (2009). Segmentation of megathrust rupture zones from fore-arc deformation patterns over hundreds to millions of years, Arauco peninsula, Chile. *Journal of Geophysical Research*, *114*, B01407. https://doi.org/10.1029/2008JB005788

Melnick, D., Moreno, M., Quinteros, J., Baez, J. C., Deng, Z., Li, S., & Oncken, O. (2017). The super-interseismic phase of the megathrust earthquake cycle in Chile. *Geophysical Research Letters*, *44*, 784–791. https://doi.org/10.1002/2016GL071845

Métois, M., Socquet, A., & Vigny, C. (2012). Interseismic coupling, segmentation and mechanical behavior of the central Chile subduction zone. *Journal of Geophysical Research*, *117*, B03406. https://doi.org/10.1029/2011JB008736

Moernaut, J., Van Daele, M., Fontijn, K., Heirman, K., Kempf, P., Pino, M., et al. (2018). Larger earthquakes recur more periodically: New insights in the megathrust earthquake cycle from lacustrine turbidite records in south-central Chile. *Earth and Planetary Science Letters*, *481*, 9–19. https://doi.org/10.1016/j.epsl.2017.10.016

Moernaut, J., Van Daele, M., Heirman, K., Fontijn, K., Strasser, M., Pino, M., et al. (2014). Lacustrine turbidites as a tool for quantitative earthquake reconstruction: New evidence for a variable rupture mode in south central Chile. *Journal of Geophysical Research: Solid Earth*, *119*, 1607–1633. https://doi.org/10.1002/2013JB010738

Mook, W. G., & van der Plicht, J. (2016). Reporting 14C activities and concentrations. *Radiocarbon*, *41*(3), 227–239. https://doi.org/10.1017/s0033822200057106

Mora, C., Comte, D., Russo, R., Gallego, A., & Mocanu, V. (2010). Aysén seismic swarm (January 2007) in southern Chile: Analysis using joint hypocenter determination. *Journal of Seismology*, *14*(4), 683–691. https://doi.org/10.1007/s10950-010-9190-y

Moreno, M., Bolte, J., Klotz, J., & Melnick, D. (2009). Impact of megathrust geometry on inversion of coseismic slip from geodetic data: Application to the 1960 Chile earthquake. *Geophysical Research Letters*, *36*, L16310. https://doi.org/10.1029/2009GL039276

Moreno, M., Melnick, D., Rosenau, M., Baez, J., Klotz, J., Oncken, O., et al. (2012). Toward understanding tectonic control on the Mw 8.8 2010 Maule Chile earthquake. *Earth and Planetary Science Letters*, *321-322*, 152–165. https://doi.org/10.1016/j.epsl.2012.01.006

Moreno, M., Melnick, D., Rosenau, M., Bolte, J., Klotz, J., Echtler, H., et al. (2011). Heterogeneous plate locking in the south–central Chile subduction zone: Building up the next great earthquake. *Earth and Planetary Science Letters*, *305*(3–4), 413–424. https://doi.org/10.1016/j.epsl.2011.03.025

Naranjo, J. A., Arenas, M., Clavero, J., & Munoz, O. (2009). Mass movement-induced tsunamis: main effects during the Patagonian Fjordland seismic crisis in Aisén (45° 25′S), Chile. *Andean Geology*, *36*(1), 137–145.

Naranjo, J. A., & Stern, C. R. (1998). Holocene explosive activity of Hudson Volcano, southern Andes. *Bulletin of Volcanology*, *59*(4), 291–306. https://doi.org/10.1007/s004450050193

Naranjo, J. A., & Stern, C. R. (2004). Holocene tephrochronology of the southernmost part (42 30′–45 S) of the Andean Southern Volcanic Zone. *Revista Geologica de Chile*, *31*(2), 224–240.

Oldfield, F., & Appleby, P. G. (1984). Empirical testing of ^{210}Pb-dating models for lake sediments. In Haworth, E. Y. & Lund, J. G. (Eds.), *Lake sediments and environmental history* (pp. 93–124). Leicester, UK: Leicester University Press

Paterson, G. A., & Heslop, D. (2015). New methods for unmixing sediment grain size data. *Geochemistry, Geophysics, Geosystems*, *16*, 4494–4506. https://doi.org/10.1002/2015GC006070

Patton, J. R., Goldfinger, C., Morey, A. E., Ikehara, K., Romsos, C., Stoner, J., et al. (2015). A 6600 year earthquake history in the region of the 2004 Sumatra-Andaman subduction zone earthquake. *Geosphere*, *11*(6), 2067–2129. https://doi.org/10.1130/ges01066.1

Pennington, W., Tutin, T. G., Cambray, R. S., & Fisher, E. M. (1973). Observations on Lake sediments using fallout ^{137}Cs as a tracer. *Nature*, *242*(5396), 324–326. https://doi.org/10.1038/242324a0

Philibosian, B., Sieh, K., Avouac, J. P., Natawidjaja, D. H., Chiang, H. W., Wu, C. C., et al. (2017). Earthquake supercycles on the Mentawai segment of the Sunda megathrust in the seventeenth century and earlier. *Journal of Geophysical Research: Solid Earth*, *122*, 642–676. https://doi.org/10.1002/2016JB013560

Pinegina, T. K., Bourgeois, J., Bazanova, L. I., Zelenin, E. A., Krasheninnikov, S. P., & Portnyagin, M. V. (2020). Coseismic coastal subsidence associated with unusually wide rupture of prehistoric earthquakes on the Kamchatka subduction zone: A record in buried erosional scarps and tsunami deposits. *Quaternary Science Reviews*, *233*, 106171. https://doi.org/10.1016/j.quascirev.2020.106171

Pouderoux, H., Proust, J.-N., Lamarche, G., Orpin, A., & Neil, H. (2012). Postglacial (after 18ka) deep-sea sedimentation along the Hikurangi subduction margin (New Zealand): Characterisation, timing and origin of turbidites. *Marine Geology*, *295-298*, 51–76. https://doi.org/10.1016/j.margeo.2011.11.002

Praet, N., Moernaut, J., Van Daele, M., Boes, E., Haeussler, P. J., Strupler, M., et al. (2017). Paleoseismic potential of sublacustrine landslide records in a high-seismicity setting (south-central Alaska). *Marine Geology*, *384*, 103–119. https://doi.org/10.1016/j.margeo.2016.05.004

Salditch, L., Stein, S., Neely, J., Spencer, B. D., Brooks, E. M., Agnon, A., & Liu, M. (2020). Earthquake supercycles and long-term fault memory. *Tectonophysics*, *774*, 228–289. https://doi.org/10.1016/j.tecto.2019.228289

Satake, K. (2015). Geological and historical evidence of irregular recurrent earthquakes in Japan. *Philosophical Transactions. Series A, Mathematical, Physical, and Engineering Sciences*, *373*(2053), 20140375. https://doi.org/10.1098/rsta.2014.0375

Satake, K., & Atwater, B. F. (2007). Long-term perspectives on giant earthquakes and tsunamis at subduction zones. *Annual Review of Earth and Planetary Sciences*, *35*(1), 349–374. https://doi.org/10.1146/annurev.earth.35.031306.140302

Sernageomin (2002). Mapa geológico de Chile: Versión digital, escala 1:1.000.000, edited, Santiago, Chile.

Simonneau, A., Chapron, E., Vannière, B., Wirth, S. B., Gilli, A., Di Giovanni, C., et al. (2013). Mass-movement and flood-induced deposits in Lake Ledro, southern Alps, Italy: Implications for Holocene palaeohydrology and natural hazards. *Climate of the Past*, *9*(2), 825–840. https://doi.org/10.5194/cp-9-825-2013

Sparkes, R., Tilmann, F., Hovius, N., & Hillier, J. (2010). Subducted seafloor relief stops rupture in South American great earthquakes: Implications for rupture behaviour in the 2010 Maule, Chile earthquake. *Earth and Planetary Science Letters*, *298*(1–2), 89–94. https://doi.org/10.1016/j.epsl.2010.07.029

Stern, C. R., & Weller, D. (2012). *A revised Age of 7430±250 14C yrs BP for the Very Large mid-Holocene Explosive H1 Eruption of the Hudson Volcano, Southern Chile* (pp. 1–2). Paper presented at 13th Chilean Geologic Congress, Antofagasta, Chile.

St-Onge, G., Chapron, E., Mulsow, S., Salas, M., Viel, M., Debret, M., et al. (2012). Comparison of earthquake-triggered turbidites from the Saguenay (Eastern Canada) and Reloncavi (Chilean margin) Fjords: Implications for paleoseismicity and sedimentology. *Sedimentary Geology*, *243-244*, 89–107. https://doi.org/10.1016/j.sedgeo.2011.11.003

St-Onge, G., Mulder, T., Piper, D. J. W., Hillaire-Marcel, C., & Stoner, J. S. (2004). Earthquake and flood-induced turbidites in the Saguenay Fjord (Québec): A Holocene paleoseismicity record. *Quaternary Science Reviews*, *23*(3–4), 283–294. https://doi.org/10.1016/j.quascirev.2003.03.001

USGS (2018). Earthquake hazards program: M 9.5–1960 great Chilean earthquake (Valdivia earthquake), https://earthquake.usgs.gov/earthquakes/eventpage/official19600522191120_30/, consulted on 9th of August, 2019.

Van Daele, M., Araya-Cornejo, C., Pille, T., Vanneste, K., Moernaut, J., Schmidt, S., et al. (2019). Distinguishing intraplate from megathrust earthquakes using lacustrine turbidites. *Geology*, *47*(2), 127–130. https://doi.org/10.1130/g45662.1

Van Daele, M., Bertrand, S., Meyer, I., Moernaut, J., Vandoorne, W., Siani, G., et al. (2016). Late Quaternary evolution of Lago Castor (Chile, 45.6°S): Timing of the deglaciation in northern Patagonia and evolution of the southern westerlies during the last 17 kyr. *Quaternary Science Reviews*, *133*, 130–146. https://doi.org/10.1016/j.quascirev.2015.12.021

Van Daele, M., Cnudde, V., Duyck, P., Pino, M., Urrutia, R., De Batist, M., & Trofimovs, J. (2014). Multidirectional, synchronously-triggered seismo-turbidites and debrites revealed by X-ray computed tomography (CT). *Sedimentology*, *61*(4), 861–880. https://doi.org/10.1111/sed.12070

Van Daele, M., Haeussler, P. J., Witter, R., Praet, N., & De Batist, M. (2019). The sedimentary record of the 2018 Anchorage earthquake in Eklutna Lake, Alaska: Calibrating the lacustrine seismograph. *Seismological Research Letters*, *91*(1), 126–141. https://doi.org/10.1785/0220190204

Van Daele, M., Meyer, I., Moernaut, J., De Decker, S., Verschuren, D., & De Batist, M. (2017). A revised classification and terminology for stacked and amalgamated turbidites in environments dominated by (hemi)pelagic sedimentation. *Sedimentary Geology*, *357*, 72–82. https://doi.org/10.1016/j.sedgeo.2017.06.007

Van Daele, M., Versteeg, W., Pino, M., Urrutia, R., & De Batist, M. (2013). Widespread deformation of basin-plain sediments in Aysén fjord (Chile) due to impact by earthquake-triggered, onshore-generated mass movements. *Marine Geology*, *337*, 67–79. https://doi.org/10.1016/j.margeo.2013.01.006

Vandekerkhove, E., Van Daele, M., Praet, N., Cnudde, V., Haeussler, P. J., De Batist, M., & Giraldclos, S. (2019). Flood-triggered versus earthquake-triggered turbidites: A sedimentological study in clastic lake sediments (Eklutna Lake, Alaska). *Sedimentology*, *67*(1), 364–389. https://doi.org/10.1111/sed.12646

Vanneste, K., Wils, K., & Van Daele, M. (2018). Probabilistic evaluation of fault sources based on paleoseismic evidence from mass-transport deposits: The example of Aysén Fjord, Chile. *Journal of Geophysical Research: Solid Earth*, *123*, 9842–9865. https://doi.org/10.1029/2018JB016289

Wells, D. L., & Coppersmith, K. J. (1994). New empirical relationships among magnitude, rupture length, rupture width, rupture area, and surface displacement. *Bulletin of the Seismological Society of America*, *84*(4), 974–1002.

Wilhelm, B., Vogel, H., & Anselmetti, F. S. (2017). A multi-centennial record of past floods and earthquakes in Valle d'Aosta, Mediterranean Italian Alps. *Natural Hazards and Earth System Sciences*, *17*(5), 613–625. https://doi.org/10.5194/nhess-17-613-2017

Wils, K., Van Daele, M., Lastras, G., Kissel, C., Lamy, F., & Siani, G. (2018). Holocene event record of Aysén Fjord (Chilean Patagonia): An interplay of volcanic eruptions and crustal and megathrust earthquakes. *Journal of Geophysical Research: Solid Earth*, *123*, 324–343. https://doi.org/10.1002/2017JB014573